掲載した論文（発表題目）	発表者氏名	発表した場所 （学会誌・雑誌等名）	発表した時期	国内・ 外の別
Role of milk fat globule-epidermal growth factor 8 in colonic inflammation and carcinogenesis,[Epub ahead of print]	Kusunoki R, Ishihara S, Tada Y, Oka A, Sonoyama H, Fukuba N, Oshima N, Moriyama I, Yuki T, Kawashima K, Ansary MMU, Tajima Y, Maruyama R, Nabika T, Kinoshita Y	J Gastroenterol.	2015 年	国外
Apoptotic Cells Ameliorate Chronic Intestinal Inflammation by Enhancing Regulatory B-cell Function,20:2308-2320	Ansary MM, Ishihara S, Oka A, Kusunoki R, Oshima N, Yuki T, Kawashima K, Maegawa H, Kashiwagi N, Kinoshita Y	Inflamm Bowel Dis.	2014 年 12 月	国外
Therapeutic Efficacy of pH-Dependent Release Formulation of Mesalazine on Active Ulcerative Colitis Resistant to Time-Dependent Release Formulation: Analysis of Fecal Calprotectin Concentration[Epub ahead of print]	Kawashima K, Ishihara S, Yuki T, Onishi K, Kushiyama Y, Fujishiro H, Miyaoka Y, Yuki M, Komazawa Y, Tanimura T, Sonoyama H, Tada Y, Kusunoki R, Oka A, Fukuba N, Oshima N, Moriyama I, Kinoshita Y	Biomed Res Int.	2014 年	国外
Regulation of anergy-related ubiquitin E3 ligase, GRAIL, in murine models of colitis and patients with Crohn's disease,49:1524-35	Mukai A, Iijima H, Hiyama S, Fujii H, Shinzaki S, Inoue T, Shiraishi E, Kawai S, Araki M, Hayashi Y, Kondo J, Mizushima T, Kanto T, Egawa S, Nishida T, Tsujii M, Takehara T.	J Gastroenterol.	2014 年・12 月	国外
Stress response protein Cirp links nflammation and tumorigenesis in colitis-associated cancer,74(21):6119-6128	Sakurai T, Kashida H, Watanabe T, Hagiwara S, Mizushima T, Iijima H, Nishida N, Higashitsuji H, Fujita J, Kudo M.	Cancer Res.	2014 年・11 月	国外
Peyer's patches play a protective role in nonsteroidal anti-inflammatory drug-induced enteropathy in mice,20:790-9	Hiyama S, Iijima H, Shinzaki S, Inoue T, Shiraishi E, Kawai S, Araki M, Kato M, Hayashi Y, Nishida T, Fujii H, Mukai A, Shibata N, Sato S, Kiyono H, Gotoh K, Motooka D, Nakamura S, Iida T, Tsujii M, Takehara T.	Inflamm Bowel Dis.	2014 年・5 月	国外
Mucin phenotype expression of gastric neuroendocrine neoplasms: analysis of histopathology and carcinogenesis,17:263-272	Domori K, Nishikura K, Ajioka Y, Aoyagi Y	Gastric Cancer	2014 年・4 月	国外
Beneficial effect of an omega-6 PUFA-rich diet in non-steroidal anti-inflammatory drug-induced mucosal damage in the murine small intestine,21(1):177-86	Ueda T, Hokari R, Higashiyama M, Yasutake Y, Maruta K, Kurihara C, Tomita K,Komoto S, Okada Y, Watanabe C, Usui S, Nagao S, Miura S.	World J Gastroenterol.	2015 年・1 月	国外
Chronic antibiotic-refractory diversion pouchitis successfully treated with leukocyteapheresis,18(6):644-5	Watanabe C, Hokari R, Miura S.	Ther Apher Dial	2014 年・12 月	国外
Magnetic resonance enterocolonography is highly detectable of erosion and redness in intestinal mucosa of patients with Crohn's disease. [Epub ahead of print]	Sato H, Tamura C, Narimatsu K, Shimizu M, Takajyo T, Yamashita M, Inoue Y,Ozaki H, Furuhashi H, Maruta K, Yasutake Y, Yoshikawa K, Watanabe C, Komoto S,Tomita K, Nagao S, Miura S, Shinmoto H, Hokari R	Gastroenterol Hepatol.	2014 年・11 月	国外

掲載した論文（発表題目）	発表者氏名	発表した場所 （学会誌・雑誌等名）	発表した時期	国内・ 外の別
Phlebosclerotic colitis that was difficult to distinguish from collagenous colitis,26(4):594-8	Hozumi H, Hokari R, Shimizu M, Maruta K, Narimatsu K, Sato H, Sato S, Ueda T, Higashiyama M, Watanabe C, Komoto S, Tomita K, Kawaguchi A, Nagao S, Miura S.	Dig Endosc.	2014年・7月	国外
Epithelial-stromal interaction via Notch signaling is essential for the full maturation of gut-associated lymphoid tissues in mice,15(12):1297-1304	Obata, Y., Kimura, S., Nakato, G., Iizuka, K., Miyagawa, Y., Nakamura1, Y., Furusawa, Y., Sugiyama, S., Suzuki, K., Ebisawa, M., Fujimura, Y., Yoshida, H., Iwanaga, T., Hase, K., Ohno, H.	EMBO R.	2014年・12月	国外

Ⅳ.　研究成果の刊行物・別刷

RESEARCH COMMUNICATION

Small intestinal stem cell identity is maintained with functional Paneth cells in heterotopically grafted epithelium onto the colon

Masayoshi Fukuda,[1,6] Tomohiro Mizutani,[1,6] Wakana Mochizuki,[1] Taichi Matsumoto,[1] Kengo Nozaki,[1] Yuriko Sakamaki,[2] Shizuko Ichinose,[2] Yukinori Okada,[3,4] Toshihiro Tanaka,[3,4] Mamoru Watanabe,[1] and Tetsuya Nakamura[5]

[1]Department of Gastroenterology and Hepatology, [2]Research Center for Medical and Dental Sciences, [3]Department of Human Genetics and Disease Diversity, [4]Bioresource Research Center, [5]Department of Advanced Therapeutics for GI Diseases, Tokyo Medical and Dental University, 113-8519 Tokyo, Japan

To develop stem cell therapy for small intestinal (SI) diseases, it is essential to determine whether SI stem cells in culture retain their tissue regeneration capabilities. By using a heterotopic transplantation approach, we show that cultured murine SI epithelial organoids are able to reconstitute self-renewing epithelia in the colon. When stably integrated, the SI-derived grafts show many features unique only to the SI but distinct from the colonic epithelium. Our study provides evidence that cultured adult SI stem cells could be a source for cell therapy of intestinal diseases, maintaining their identity along the gastrointestinal tract through an epithelium-intrinsic mechanism.

Supplemental material is available for this article.

Received May 19, 2014; revised version accepted July 23, 2014.

Recent advances have enabled long-term culture and expansion of epithelial stem cells of the small intestine (SI) and colon in vitro (Ootani et al. 2009; Sato et al. 2009, 2011a; Jung et al. 2011). With the advent of such technologies, there has emerged a growing interest in the use of these cultured adult stem cells in replacement therapy for intestinal epithelial injuries. We demonstrated previously that *Lgr5*$^+$ colonic stem cells are able to regenerate normal epithelia when expanded in culture and transplanted onto a damaged colon in mice (Yui et al. 2012). To extend such an approach to SI diseases, it is imperative to test whether SI stem cells in culture retain their tissue regeneration capabilities.

[*Keywords*: small intestinal stem cell; transplantation; stem cell niche; Paneth cell; regenerative medicine]
[6]**These authors contributed equally to this study.**
Corresponding author: nakamura.gast@tmd.ac.jp
Article is online at http://www.genesdev.org/cgi/doi/10.1101/gad.245233.114.

Despite common features, epithelia of the SI and colon show many differences. The former builds protruding villus structures that are connected to glandular structures called crypts, whereas the latter only forms crypts (Sancho et al. 2004). They also differ in their cellular components, as represented by Paneth cells that reside only in the SI and play a role in innate immunity (Clevers and Bevins 2013). Such heterogeneity may result from organ-specific, developmentally acquired programs in respective epithelium and environmental cues from the surrounding nonepithelial components in respective tissues. However, how epithelium-intrinsic and epithelium-extrinsic factors contribute to the establishment and maintenance of intestinal identity remains unclear.

In this study, by employing the cell transplantation technique developed in our laboratory, we investigated whether cultured SI stem cells are capable of regenerating epithelia in vivo and how adult SI epithelial cells behave when heterotopically transplanted onto the colon (Fig. 1A).

Results and Discussion

To obtain denuded colonic regions that would potentially allow engraftment of transplanted SI cells, we developed a new mouse recipient model of colonic mucosal injury. The distal colonic lumen was exposed to a chelating agent, and then mechanical epithelial abrasion was performed. This procedure yielded mucosal injuries along the whole circumference of the distal colonic segment (Fig. 1B). Histology showed that the epithelial layer was largely stripped, with small, discrete epithelial elements left behind, whereas the underlying tissue remained almost intact (Fig. 1C). Shortly thereafter, epithelial repair occurred rapidly and was nearly completed within 4 wk (Supplemental Fig. S1).

SI epithelial cells were isolated from adult *EGFP* transgenic mice (Okabe et al. 1997) and cultured for 7 d as stem cell-containing organoids (Sato et al. 2009). They were then collected and instilled into the colonic lumen of syngeneic, immunocompetent wild-type recipients in which colonic epithelial injury was generated beforehand (day 1). One day after transplantation (day 2), we found that EGFP$^+$ cells showed a scattered distribution on the recipient colon (Fig. 1D–D″). The EGFP$^+$ areas were mostly composed of a cluster of cells, implying that the transplanted cells adhered to the tissue still partly preserving their organoid structure (Fig. 1D′,D″). Histological analysis revealed a variety of appearances in those areas. Some displayed a convoluted, continuous lining of EGFP$^+$ cells, a part of which directly contacted with the denuded tissue (Fig. 1E). In other areas, the EGFP$^+$ cells covered the luminal surface as a flat lining of single-layered cells (Fig. 1F). The grafted cells were shown to remain as epithelial cells, since they were all positive for Cdh1 (Fig. 1E″,F″). Fordham et al. (2013) recently reported that SI epithelial progenitors of fetal origin are able to grow as fetal enterospheres (FEnSs) in vitro. When transplanted

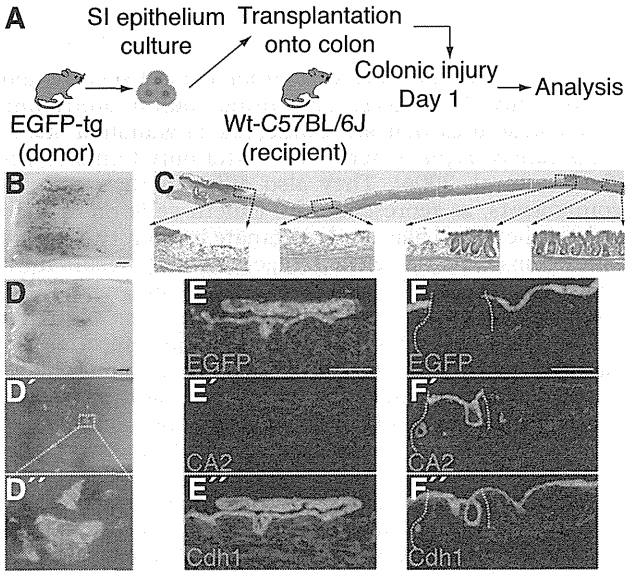

Figure 1. Cultured SI epithelial cells repopulate onto injured colons upon transplantation. (*A*) Experimental protocol. (*B*) Colonic injury model used in the present study. Stereoscopic image of the distal colon immediately after generation of injury. (*C*) H&E staining of the longitudinally sectioned colon shown in *B*. The anal side is shown on the *left*, and the oral side is on the *right*. High-power views of areas in dotted boxes are shown *below*. (*D*) Recipient colon at 1 d after transplantation. Stereoscopic image (*D*) and its fluorescent (EGFP) view (D′). High-power view of the dotted rectangle is shown in D″. (*E,F*) Histological analysis of the graft shown in *D*. EGFP fluorescence (*E,F*), immunohistochemistry for CA2 (*E′,F′*) and Cdh1 (*E″,F″*) are shown. The *top* two images (*E,E′,F,F′*) are the results sequentially obtained from the same section, and the *bottom* images (*E″,F″*) are their adjacent sections. Note that the antigen retrieval procedure before immunostaining completely clears endogenous EGFP signals. Fluorescent images are presented with DAPI staining. White dotted lines show borders between EGFP$^+$ and EGFP$^-$ epithelia. Bars: *B–D*, 1 mm; *E,F*, 100 μm.

onto the adult colon, FEnS-derived cells showed plasticity in regard to their cell fate by expressing CA2, a marker protein of colonic epithelium (Fordham et al. 2013). Interestingly, the EGFP$^+$ areas derived from adult SI cells in this study did not show obvious expression of CA2 (Fig. 1E′). This was clearly visible in contrast to its exclusive expression in the EGFP$^-$ epithelium of recipient origin, which survived the damage and intervened in two separate EGFP$^+$ areas of donor origin (Fig. 1F′). It is thus shown that adult SI epithelial cells in culture are able to repopulate onto the colon in a manner different from that of fetal SI progenitor cells.

At 2 wk post-transplantation (Fig. 2A), EGFP$^+$ cells displayed intricate structures containing many invaginations extending downward (Fig. 2B). They were still devoid of CA2 expression (Fig. 2B′). We found that expression of CDX2, an intestine-specific transcription factor that plays important roles in regional maintenance of gastrointestinal epithelial cells (Silberg et al. 2000; Gao et al. 2009), was clearly demarcated by the borders between EGFP$^-$ and EGFP$^+$ epithelia (Fig. 2B″). This recapitulated its high expression in the SI and low abundance in the distal colon of adult mice (Silberg et al. 2000), suggesting that adult SI-derived donor cells retain their original identity.

EGFP$^+$ areas contained Ki67$^+$ cells at the lower compartment of invaginations, indicating that SI-derived cells proliferated actively in the colon (Fig. 2C). Differentiated cell types—such as Goblet cells, enteroendocrine cells, and sucrase isomaltase (SIase)-expressing absorptive cells of the SI—were also detected (Fig. 2D–F). In addition, lysozyme$^+$ Paneth-like cells were detected exclusively in the EGFP$^+$ epithelium (Fig. 2G). These results suggested that the transplanted cells are able to reconstitute self-renewing epithelia of SI phenotype in vivo even after being heterotopically engrafted. The retention of SI phenotype is unlikely to be a feature acquired through the culture process, as we obtained similar results when freshly isolated SI crypts were immediately transplanted and then recipients were analyzed at 2 wk (Supplemental Fig. S2).

At 4 wk, the EGFP$^+$ epithelia were found to be stably incorporated in the colon (Fig. 3A). Within some but not all areas of grafts, there emerged structures reminiscent of typical architecture of the SI epithelium. Cells constituting finger-like projections were directly linked to flask-shaped, crypt-like invaginations (Fig. 3A″). The tissue lying beneath the EGFP$^+$ epithelium contained a number of cellular components of recipient origin, such as immune cells (CD3$^+$ and F4/80$^+$) and CD31$^+$ blood vessel endothelial cells (Supplemental Fig. S3), indicating that epithelial and nonepithelial elements of different origins cooperatively assembled into the crypt/villus structure. A recent report demonstrated that the villus formation occurs as a result of stepwise differentiation of the outer smooth muscle layers, which restricts the planar expansion of growing epithelium/mesenchyme and thereby generates protrusions into the lumen (Shyer et al. 2013). This, however, described the process of villi specification in fetal stages and may not account for our data in which epithelial reorganization occurred in fully mature adult colons. Other reports showed that the epithelial–mesenchymal cross-talk regulates the patterning of villi through a mechanism involving PDGFRα-expressing mesenchymal cells (Madison et al. 2005; Walton et al. 2012). In our attempts, however, the clusters of PDGFRα$^+$ cells, which were reported to emerge at the

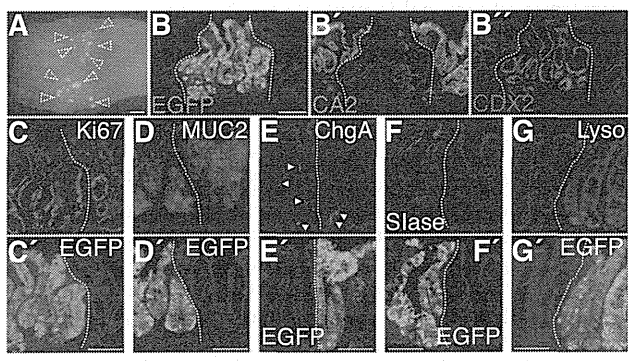

Figure 2. SI epithelial cells reconstitute self-renewing epithelia of SI phenotype in the colon. (*A*) Recipient colon at 2 wk post-transplantation. Stereoscopic image overlaid with EGFP fluorescence. Dotted arrowheads show EGFP$^+$ grafts. (*B*) EGFP fluorescence of a section obtained from the tissue shown in *A*. The same section was double-stained for CA2 (*B′*) and CDX2 (*B″*). (*C–G*) Immunofluorescence for Ki67 (*C*), MUC2 (*D*), ChgA (*E*), SIase (*F*), and lysozyme (*G*). Arrowheads point to ChgA$^+$ cells. Images of adjacent sections stained with GFP-specific antibody (*C′,G′*) or endogenous EGFP fluorescence of the same sections (*D′,E′,F′*) are shown at the *bottom*. All fluorescent images are presented with DAPI staining. White dotted lines show borders between EGFP$^+$ and EGFP$^-$ epithelia. Bars: *A*, 1 mm; *B–G*, 100 μm.

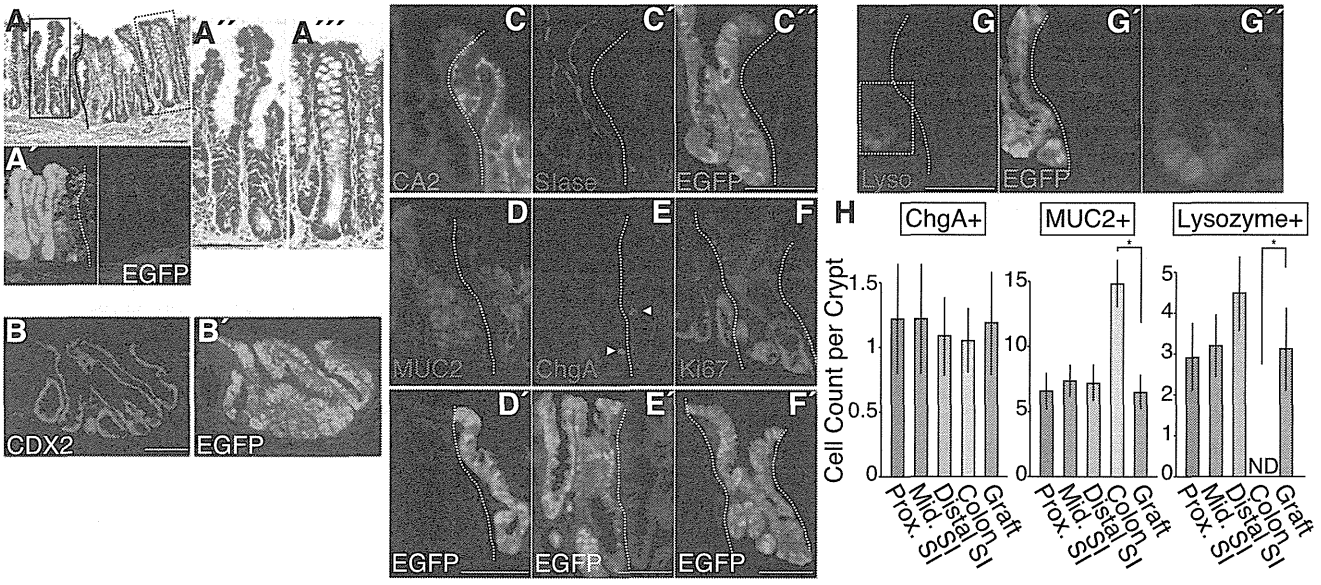

Figure 3. SI phenotypes are preserved in stably integrated SI-derived grafts at 4 wk post-transplantation. (*A*) Histological analysis of the recipient colon at 4 wk post-transplantation. H&E staining of a section (*A*) and its EGFP fluorescence (*A′*). High-power views of areas in dotted boxes in *A* are shown as *A″* and *A‴*. (*B*,*B′*) Immunostaining for CDX2 (*B*) and an adjacent section stained with GFP-specific antibody (*B′*). (*C*–*C″*) Section double-stained with CA2 (*C*) and SIase (*C′*) is presented, with the adjacent section stained with GFP-specific antibody (*C″*). (*D*–*G*) Immunofluorescence for MUC2 (*D*), ChgA (*E*), Ki67 (*F*), and lysozyme (*G*). Arrowheads point to ChgA$^+$ cells. Images of adjacent sections stained with GFP-specific antibody (*F′*) or those of endogenous EGFP fluorescence of the same sections (*D′*,*E′*,*G′*) are also shown. High-power view of the area within the dotted box or rectangle in *G* is shown in *G″*. (*H*) Quantification of cellular components. Mean cell counts of ChgA$^+$, MUC2$^+$, or lysozyme$^+$ cells per crypt–villus or crypt unit are presented for the proximal (Prox. SI), middle (Mid. SI), and distal (Distal SI) SI; the colon; and EGFP$^+$ grafts (Graft). Error bars indicate SEM. (*) $P < 0.05$. All fluorescent images are shown with DAPI staining. Dotted lines indicate borders between EGFP$^+$ and EGFP$^-$ epithelia. Bars: *A*–*G*, 100 μm.

site of villus formation (Walton et al. 2012), were not detectable in subepithelia of any grafts (data not shown). This suggests that some additional mechanisms might be involved in morphogenesis of the villus-like structures in this artificial situation in which epithelial and nonepithelial components of different origins coexist.

EGFP$^+$ epithelial cells at 4 wk retained a higher expression of CDX2 than the surrounding recipient colon (Fig. 3B). They were negative for CA2 expression (Fig. 3C), which was in sharp contrast to the inverted expression pattern of SIase (Fig. 3C′). Goblet cells (Fig. 3D), enteroendocrine cells (Fig. 3E), and Ki67$^+$ proliferating cells (Fig. 3F) were present in the EGFP$^+$ epithelium. In addition, lysozyme$^+$ Paneth cells were found at the bottom-most regions of the EGFP$^+$ crypts, as in physiological SI epithelium (Fig. 3G). Even 4 mo after transplantation, multidifferentiation and self-renewal capabilities of the grafted cells remained stable. The EGFP$^+$ epithelia formed distinguishable crypt/villus structures that contained cells of multilineages as well as proliferating cells (Supplemental Fig. S4). When quantitative analysis was performed with the grafts at 4 wk post-transplantation, the numbers of Goblet cells (MUC2$^+$) and Paneth cells (lysozyme$^+$) in EGFP$^+$ areas showed a significant difference from those in normal colonic epithelium. Rather, they were comparable with those in the SI epithelium from which the grafted cells originated (Fig. 3H).

To verify this observation at the molecular level, gene expression profiles of EGFP$^+$ epithelium in the graft (4 wk post-transplantation) and control colonic epithelium were assessed by laser capture microdissection and microarray analysis (Supplemental Fig. S5). Comparative analysis of the data identified 452 probe sets (see the Supplemental Material) that show enrichment in either of the two data sets by more than threefold (Supplemental Table S1). Of note, among those that are highly enriched in the graft are many genes known to be expressed in Paneth cells, such as *α-defensins* (Amid et al. 2009; Ouellette 2011) and *lyz1* (Keshav 2006). Genes involved in transporter activity are also expressed differently in these two tissues. For example, compared with the colonic epithelium, the graft epithelium showed higher expression of genes encoding solute carrier (SLC) family members (*slc26a6* and *slc7a9*) and non-SLC transporters (*fabp1* and *rbp2*) but lower expression of other SLC genes (*slc20a1*, *slc26a2*, *slc35a1*, *slc40a1*, and *slc6a14*). Differential expression levels of these transporter genes between these two samples are consistent with their differentially regulated expression patterns in the SI and colon in vivo (Anderle et al. 2005). In addition, the genes enriched in the graft contain *pdx1* (Offield et al. 1996) and *gata4* (Bosse et al. 2006; Middendorp et al. 2014), both of which encode transcription factors that control region-specific gene expression in the SI. These data suggested that, even in the colonic milieu, the graft epithelium retains their commitment to the SI phenotype with preservation of functional Paneth cells and expression of a particular set of SI-specific genes.

Multipotent, rapidly cycling stem cells known to express Lgr5 reside at the base of crypts in both the SI and colon (Barker et al. 2007). The Lgr5$^+$ SI stem cells are morphologically characterized as crypt base columnar (CBC) cells interspersed with Paneth cells (Sato et al. 2011b). In contrast, the cells of CBC phenotype are not present in the colon, where classical Paneth cells are absent. By transmission electron microscopy, we were able to document that a crypt of SI phenotype, which contained

Paneth-like cells with discernible secretory granules, was located immediately adjacent to a "goblet cell-rich" crypt of colonic phenotype on the contiguous mesenchyme (Fig. 4A). When the neighboring section was examined at a higher magnification, a slender columnar cell wedged between two Paneth-like cells was visible, which resembled the CBC cells in the SI (Fig. 4A′). Stem cells in the grafted areas were examined further. Among several genes that label Lgr5$^+$ SI stem cells (van der Flier et al. 2009b; Hao et al. 2012; Koo et al. 2012; Munoz et al. 2012), *Olfm4*, a gene encoding a secreted protein of the Olfactomedin family, is known to mark SI but not colonic stem cells in mice (van der Flier et al. 2009a,b). When boundary areas were examined by in situ hybridization (ISH), *Olfm4* was found to be present at the bottom of EGFP$^+$ crypts but not in EGFP$^-$ areas (Fig. 4B). These results suggest that crypt base cells in the graft maintain the structural and functional properties of adult SI stem cells.

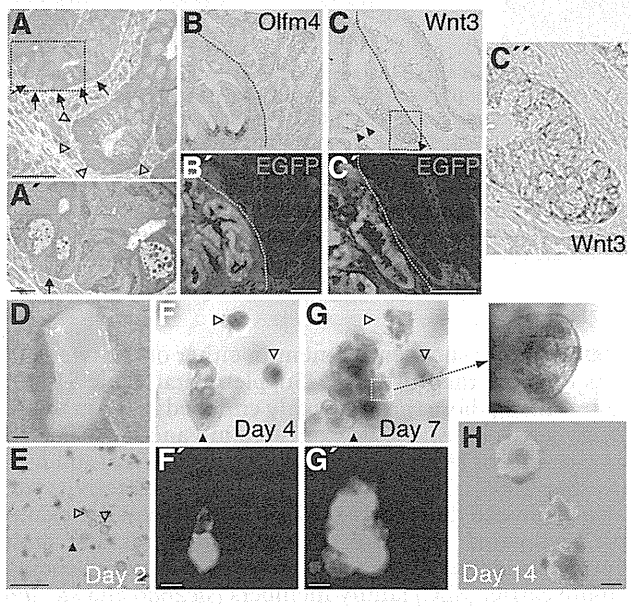

Figure 4. SI-derived grafts contain stem cell compartments of SI phenotype. (*A*) Transmission electron microscopy analysis for graft at 4 wk post-transplantation. Crypt of SI phenotype (arrows) located immediately adjacent to that of colonic phenotype (arrowheads). High-magnification view of a neighboring section corresponding to the area within the dotted rectangle is shown in *A*′. The arrow points to a slender columnar cell wedged between Paneth-like cells. (*B*) In situ hybridization for *Olfm4* on tissue 4 wk post-transplantation. (*B*′) An adjacent section immunostained for EGFP is also shown. (*C*) In situ hybridization for *Wnt3*. (*C*′) An adjacent section immunostained for EGFP is shown. (*C*″) A high-power view of the area within the dotted box or rectangle is also presented. (*D*) Portion of recipient colon at 8 wk post-transplantation from which epithelia were reisolated. The epithelium was then cultured in medium supplemented with EGF, Noggin, and R-spondin1 but without Wnt3a. (*E*) Image of reisolated cells 1 d after the start of culture (day 2). Merged image of phase-contrast and EGFP fluorescence views. (*F,G*) Images of culture on day 4 (*F*) and day 7 (*G*). Phase-contrast images (*F,G*) and their EGFP signals (*F′,G′*) are shown. A high-power view of the area in the dotted square is shown at the *right*. A filled triangle and open triangles in *E*, *F*, and *G* denote the identical structures tracked throughout the experiment. (*H*) Merged image of phase-contrast and EGFP fluorescence views of day 14 organoids grown after passage. All fluorescent images of fixed tissues are shown with DAPI staining. Dotted lines indicate borders between EGFP$^+$ and EGFP$^-$ epithelia. Bars: *A*, 50 μm; *A*′, 10 μm; *B,C,F–H*, 100 μm; *E*, 500 μm; *D*, 1 mm.

Both epithelial and nonepithelial cells express Wnts and constitute a niche for Lgr5$^+$ stem cells (Gregorieff et al. 2005; Sato et al. 2011b). In the SI, Paneth cells express many Wnts and thereby function as the major component of "epithelial niche" for adjacent Lgr5$^+$ stem cells (Sato et al. 2011b). Among many Wnts, Wnt3 is considered to be a pivotal niche factor, as its depletion results in the growth impairment of SI epithelial cells in vitro (Farin et al. 2012). Such function of Wnt3 may be predominant in the SI, as it is expressed in Paneth cells but not at a detectable level in the colon (Farin et al. 2012). When examined by ISH, *Wnt3* was shown to be expressed only at the base of EGFP$^+$ crypts (Fig. 4C), suggesting that these Wnt3-producing cells—most likely Paneth cells—are functional as a part of the stem cell niche in the grafts of SI origin.

The SI epithelium is known to behave differently from the colonic one in in vitro culture. Since Paneth cells serve as a local source of Wnts, SI cells grow asymmetrically, building many protrusions that resemble in vivo crypt structures (Sato et al. 2009). In contrast, due to the absence of Paneth cells, colonic cells require exogenous Wnts in culture (Jung et al. 2011; Sato et al. 2011a; Yui et al. 2012). To assess more directly the functional properties of graft cells, epithelia were isolated from a recipient colon at 2 mo post-transplantation (Fig. 4D) and cultured in the absence of Wnt3. While EGFP$^+$ graft cells and EGFP$^-$ colonic cells both survived as simple spherical cysts for the first few days (Fig. 4E,4F), EGFP$^-$ cysts eventually collapsed and degenerated (Fig. 4G), reflecting the absolute dependence of colonic cell culture on exogenous Wnts. On the other hand, EGFP$^+$ cysts matured into organoids of SI phenotype (Fig. 4G) and could be further propagated (Fig. 4H). Notably, the EGFP$^+$ organoids generated many crypt-like budding structures harboring granule-rich Paneth cells (Fig. 4G). These in vitro data clearly show the continued presence of SI stem cells in the graft, which give rise to competent Paneth cells that in turn produce sufficient niche signals for stem cells.

In summary, we show here that cultured adult SI stem cells are capable of reconstituting epithelial tissues of SI phenotype in vivo, with functional Paneth cells that serve as a niche component. In addition to previous studies on adult colon stem cells (Yui et al. 2012) and fetal SI progenitor cells (Fordham et al. 2013), this study adds the adult SI stem cells to the list of transplantable cells for treatment of intestinal diseases. Moreover, our study highlights the epithelium-intrinsic program that allows for maintenance of organ-specific stem cell properties in adult intestines.

Materials and methods

Mice

Six-wk-old to 10-wk-old *EGFP* transgenic mice of C57BL6 background (Okabe et al. 1997) were used as a source for donor cells. C57BL6 mice of 6–10 wk of age were used as recipients. All animal experiments were performed with the approval of the Institutional Animal Care and Use Committee of Tokyo Medical and Dental University.

Isolation and culture of SI crypts

SI crypts were isolated from *EGFP* transgenic mice as described previously (Sato et al. 2009). Epithelial reisolation from the recipient colon was

performed according to the method previously described for colonic crypt isolation (Yui et al. 2012). A total of 300 crypts was suspended in 30 μL of Matrigel (BD Biosciences) and placed in 24-well plates. After polymerization, 500 μL of advanced DMEM/F12 containing 500 ng/mL mRspo1 (R&D Systems), 20 ng/mL mEGF (Peprotech), and 100 ng/mL mNoggin (R&D Systems) was added to each well. The medium was changed every 3 d until the following use of cultured cells for transplantation experiments.

Generation of colonic epithelial injury

C57BL6 mice were anesthetized with an intraperitoneal injection of tribromoethanol solution (0.5 mg/g body). Topical exposure of the colonic mucosa to ethylenedinitrilo tetraacetic acid (EDTA) was achieved by the use of a thin catheter (1 mm in diameter) that was equipped with two small balloons (Supplemental Fig. S1). The catheter was inserted 1 cm via a transanal approach, and the balloons were inflated with air to hold them in place. Another thin catheter was inserted, and the luminal space between two balloons was filled with 500 μL of 500 mM EDTA/phosphate-buffered saline (PBS). After 2 min of exposure, the lumen was emptied by aspiration of the EDTA solution. After deflating the balloons, both catheters were removed out of the colon. Epithelial abrasion was performed with an electric brush (Supplemental Fig. S1). The head of the device was inserted 1 cm into the colon, and a rotational movement was given for 1 min to gently scratch the entire circumference of the luminal surface.

Transplantation

Typically, from a single mouse, our isolation procedure liberates as many SI crypts as can be seeded into ~200 wells on 24-well plates. For transplantation, SI organoids were grown for 7 d and released from Matrigel using cell recovery solution (Corning). Cell suspension was made without further dissociation of the structure, so the organoids equivalent to those harvested from 200 wells were suspended in 2 mL of a diluted Matrigel/PBS (1:10) solution. Two-hundred microliters of cell suspension was instilled into the colonic lumen of each recipient mouse by using a syringe and a thin flexible catheter 4 cm in length and 2 mm in diameter. After infusion, the anal verge was sutured and left for 12 h to prevent luminal contents from being excreted immediately. After the procedure, mice were maintained as usual before they were sacrificed and analyzed.

Stereomicroscopy, histology, and immunohistochemistry

Whole distal colons of recipients and their fluorescence were imaged using a fluorescence stereomicroscope system (MVX10, Olympus). Protocols for histology and immunohistochemistry and the antibodies used in this study are included in the Supplemental Material. Fluorescent images of sections were acquired using a DeltaVision system (Applied Precision). For quantification of cellular components, sections of the proximal, middle, and distal SI, colon, and $EGFP^+$ grafts were subjected to immunohistochemistry for ChgA, MUC2, or lysozyme. Thirty crypt–villus units or crypt units (colon), originating from three independent recipients or normal controls, were analyzed. The numbers of $ChgA^+$, $MUC2^+$, or $lysozyme^+$ cells were counted and presented as mean cell counts per crypt–villus or crypt unit. Statistical significance was determined by Student's *t*-test ($P < 0.05$).

Transmission electron microscopy

Recipient colons were cut at the area of $EGFP^+$ grafts so that the cutting plane would contain $EGFP^+$ epithelium. Pieces of tissues were fixed with 2.5% glutaraldehyde in 0.1 M PBS for 2 h, washed overnight at 4°C in the same buffer, post-fixed with 1% OsO_4 buffered with 0.1 M PBS for 2 h, dehydrated in a graded series of ethanol, and embedded in Epon 812. Ultrathin (90-nm) sections were first collected on single-hole meshes in order to acquire low-magnification images that contained crypts of SI and colonic phenotypes located next to each other. Next, the adjacent sections were collected on copper grids to obtain a magnified view of those areas. Sections were double-stained with uranyl acetate and lead citrate and then examined with a transmission electron microscope (H-7100, Hitachi).

ISH

ISH for *Olfm4* and *Wnt3* was performed essentially as described previously (Gregorieff et al. 2005; Sato et al. 2011b). A pcDNA3 plasmid containing a cDNA fragment of mouse *Olfm4* (nucleotides 259–651; GenBank accession no. NM001030294.1) was constructed. A plasmid containing a fragment of mouse *Wnt3* (Gregorieff et al. 2005; Sato et al. 2011b) was a kind gift from Professor Hans Clevers (Hubrecht Institute). Single-stranded, digoxigenin-labeled RNA probes were generated by in vitro transcription system (Roche). Frozen sections were rehydrated, treated with HCl, digested in proteinase K solution, post-fixed, treated in acetic anhydride solution, and hybridized overnight at 68°C with probes. After extensive rinsing and washing, sections were then subjected to the immunohistochemistry by using alkaline phosphatase–conjugated anti-digoxigenin antibody (Roche). Sections were then reacted with a nitroblue tetrazolium/5-bromo-4-chloro-3-indolyl phosphate solution for color development. Image were acquired on a microscope (BZ-8000, Keyence).

Comparison of gene expression profiles

Protocols for laser capture microdissection and microarray analysis can be found in the Supplemental Material. The microarray data were deposited into Gene Expression Omnibus (GEO) under the accession number GSE59410.

Acknowledgments

We thank Professor Hans Clevers and Dr. Henner Farin (Hubrecht Institute) for technical assistance, and Lesa Thompson for comments on the manuscript. This study was supported by Ministry of Education, Culture, Sports, Science, and Technology (MEXT) KAKENHI (grant no. 24112508), Japan Society for the Promotion of Science (JSPS) KAKENHI (25670106, 24390186, and 22229005), the Regenerative Medicine Realization Base Network Program from the Japan Science and Technology Agency, and Health and Labour Sciences Research Grants for research on Intractable Diseases from the Ministry of Health, Labor, and Welfare of Japan.

References

Amid C, Rehaume LM, Brown KL, Gilbert JG, Dougan G, Hancock RE, Harrow JL. 2009. Manual annotation and analysis of the defensin gene cluster in the C57BL/6J mouse reference genome. *BMC Genomics* **10:** 606.

Anderle P, Sengstag T, Mutch DM, Rumbo M, Praz V, Mansourian R, Delorenzi M, Williamson G, Roberts MA. 2005. Changes in the transcriptional profile of transporters in the intestine along the anterior-posterior and crypt–villus axes. *BMC Genomics* **6:** 69.

Barker N, van Es JH, Kuipers J, Kujala P, van den Born M, Cozijnsen M, Haegebarth A, Korving J, Begthel H, Peters PJ, et al. 2007. Identification of stem cells in small intestine and colon by marker gene Lgr5. *Nature* **449:** 1003–1007.

Bosse T, Piaseckyj CM, Burghard E, Fialkovich JJ, Rajagopal S, Pu WT, Krasinski SD. 2006. Gata4 is essential for the maintenance of jejunal-ileal identities in the adult mouse small intestine. *Mol Cell Biol* **26:** 9060–9070.

Clevers HC, Bevins CL. 2013. Paneth cells: maestros of the small intestinal crypts. *Annu Rev Physiol* **75:** 289–311.

Farin, H.F., Van Es, J.H., and Clevers, H. 2012. Redundant sources of Wnt regulate intestinal stem cells and promote formation of Paneth cells. *Gastroenterology* **143:** 1518–1529.e7.

Fordham RP, Yui S, Hannan NR, Soendergaard C, Madgwick A, Schweiger PJ, Nielsen OH, Vallier L, Pedersen RA, Nakamura T, et al. 2013. Transplantation of expanded fetal intestinal progenitors contributes to colon regeneration after injury. *Cell Stem Cell* **13:** 734–744.

Gao N, White P, Kaestner KH. 2009. Establishment of intestinal identity and epithelial-mesenchymal signaling by Cdx2. *Dev Cell* **16:** 588–599.

Gregorieff A, Pinto D, Begthel H, Destree O, Kielman M, Clevers H. 2005. Expression pattern of Wnt signaling components in the adult intestine. *Gastroenterology* **129:** 626–638.

Hao HX, Xie Y, Zhang Y, Charlat O, Oster E, Avello M, Lei H, Mickanin C, Liu D, Ruffner H, et al. 2012. ZNRF3 promotes Wnt receptor turnover in an R-spondin-sensitive manner. *Nature* **485:** 195–200.

Jung P, Sato T, Merlos-Suarez A, Barriga FM, Iglesias M, Rossell D, Auer H, Gallardo M, Blasco MA, Sancho E, et al. 2011. Isolation and in vitro expansion of human colonic stem cells. *Nat Med* **17:** 1225–1227.

Keshav S. 2006. Paneth cells: leukocyte-like mediators of innate immunity in the intestine. *J Leukoc Biol* **80:** 500–508.

Koo BK, Spit M, Jordens I, Low TY, Stange DE, van de Wetering M, van Es JH, Mohammed S, Heck AJ, Maurice MM, et al. 2012. Tumour suppressor RNF43 is a stem-cell E3 ligase that induces endocytosis of Wnt receptors. *Nature* **488:** 665–669.

Madison BB, Braunstein K, Kuizon E, Portman K, Qiao XT, Gumucio DL. 2005. Epithelial hedgehog signals pattern the intestinal crypt–villus axis. *Development* **132:** 279–289.

Middendorp S, Schneeberger K, Wiegerinck CL, Mokry M, Akkerman RD, van Wijngaarden S, Clevers H, Nieuwenhuis EE. 2014. Adult stem cells in the small intestine are intrinsically programmed with their location-specific function. *Stem Cells* **32:** 1083–1091.

Munoz J, Stange DE, Schepers AG, van de Wetering M, Koo BK, Itzkovitz S, Volckmann R, Kung KS, Koster J, Radulescu S, et al. 2012. The Lgr5 intestinal stem cell signature: robust expression of proposed quiescent '+4' cell markers. *EMBO J* **31:** 3079–3091.

Offield MF, Jetton TL, Labosky PA, Ray M, Stein RW, Magnuson MA, Hogan BL, Wright CV. 1996. PDX-1 is required for pancreatic outgrowth and differentiation of the rostral duodenum. *Development* **122:** 983–995.

Okabe M, Ikawa M, Kominami K, Nakanishi T, Nishimune Y. 1997. 'Green mice' as a source of ubiquitous green cells. *FEBS Lett* **407:** 313–319.

Ootani A, Li X, Sangiorgi E, Ho QT, Ueno H, Toda S, Sugihara H, Fujimoto K, Weissman IL, Capecchi MR, et al. 2009. Sustained in vitro intestinal epithelial culture within a Wnt-dependent stem cell niche. *Nat Med* **15:** 701–706.

Ouellette AJ. 2011. Paneth cell α-defensins in enteric innate immunity. *Cell Mol Life Sci* **68:** 2215–2229.

Sancho E, Batlle E, Clevers H. 2004. Signaling pathways in intestinal development and cancer. *Annu Rev Cell Dev Biol* **20:** 695–723.

Sato T, Vries RG, Snippert HJ, van de Wetering M, Barker N, Stange DE, van Es JH, Abo A, Kujala P, Peters PJ, et al. 2009. Single Lgr5 stem cells build crypt–villus structures in vitro without a mesenchymal niche. *Nature* **459:** 262–265.

Sato T, Stange DE, Ferrante M, Vries RG, Van Es JH, Van den Brink S, Van Houdt WJ, Pronk A, Van Gorp J, Siersema PD, et al. 2011a. Long-term expansion of epithelial organoids from human colon, adenoma, adenocarcinoma, and Barrett's epithelium. *Gastroenterology* **141:** 1762–1772.

Sato T, van Es JH, Snippert HJ, Stange DE, Vries RG, van den Born M, Barker N, Shroyer NF, van de Wetering M, Clevers H. 2011b. Paneth cells constitute the niche for Lgr5 stem cells in intestinal crypts. *Nature* **469:** 415–418.

Shyer AE, Tallinen T, Nerurkar NL, Wei Z, Gil ES, Kaplan DL, Tabin CJ, Mahadevan L. 2013. Villification: how the gut gets its villi. *Science* **342:** 212–218.

Silberg DG, Swain GP, Suh ER, Traber PG. 2000. Cdx1 and cdx2 expression during intestinal development. *Gastroenterology* **119:** 961–971.

van der Flier LG, Haegebarth A, Stange DE, van de Wetering M, Clevers H. 2009a. OLFM4 is a robust marker for stem cells in human intestine and marks a subset of colorectal cancer cells. *Gastroenterology* **137:** 15–17.

van der Flier LG, van Gijn ME, Hatzis P, Kujala P, Haegebarth A, Stange DE, Begthel H, van den Born M, Guryev V, Oving I, et al. 2009b. Transcription factor achaete scute-like 2 controls intestinal stem cell fate. *Cell* **136:** 903–912.

Walton KD, Kolterud A, Czerwinski MJ, Bell MJ, Prakash A, Kushwaha J, Grosse AS, Schnell S, Gumucio DL. 2012. Hedgehog-responsive mesenchymal clusters direct patterning and emergence of intestinal villi. *Proc Natl Acad Sci* **109:** 15817–15822.

Yui S, Nakamura T, Sato T, Nemoto Y, Mizutani T, Zheng X, Ichinose S, Nagaishi T, Okamoto R, Tsuchiya K, et al. 2012. Functional engraftment of colon epithelium expanded in vitro from a single adult $Lgr5^+$ stem cell. *Nat Med* **18:** 618–623.

nature COMMUNICATIONS

ARTICLE

Received 25 Sep 2013 | Accepted 21 Mar 2014 | Published 10 Apr 2014

DOI: 10.1038/ncomms4704

Generation of colonic IgA-secreting cells in the caecal patch

Kazunori Masahata[1,2], Eiji Umemoto[1,3], Hisako Kayama[1,3], Manato Kotani[4], Shota Nakamura[5], Takashi Kurakawa[1], Junichi Kikuta[4], Kazuyoshi Gotoh[5], Daisuke Motooka[5], Shintaro Sato[6], Tomonori Higuchi[7], Yoshihiro Baba[8], Tomohiro Kurosaki[8], Makoto Kinoshita[1,3], Yosuke Shimada[1], Taishi Kimura[1], Ryu Okumura[1], Akira Takeda[1], Masaru Tajima[9], Osamu Yoshie[7], Masahiro Fukuzawa[2], Hiroshi Kiyono[3,6], Sidonia Fagarasan[10], Tetsuya Iida[5,11], Masaru Ishii[3,4] & Kiyoshi Takeda[1,3]

Gut-associated lymphoid tissues are responsible for the generation of IgA-secreting cells. However, the function of the caecal patch, a lymphoid tissue in the appendix, remains unknown. Here we analyse the role of the caecal patch using germ-free mice colonized with intestinal bacteria after appendectomy. Appendectomized mice show delayed accumulation of IgA^+ cells in the large intestine, but not the small intestine, after colonization. Decreased colonic IgA^+ cells correlate with altered faecal microbiota composition. Experiments using photoconvertible Kaede-expressing mice or adoptive transfer show that the caecal patch IgA^+ cells migrate to the large and small intestines, whereas Peyer's patch cells are preferentially recruited to the small intestine. IgA^+ cells in the caecal patch express higher levels of CCR10. Dendritic cells in the caecal patch, but not Peyer's patches, induce CCR10 on cocultured B cells. Thus, the caecal patch is a major site for generation of IgA-secreting cells that migrate to the large intestine.

[1] Laboratory of Immune Regulation, Department of Microbiology and Immunology, Graduate School of Medicine, WPI Immunology Frontier Research Center, Osaka University, Suita, Osaka 565-0871, Japan. [2] Department of Pediatric Surgery, Graduate School of Medicine, Osaka University, Suita, Osaka 565-0871, Japan. [3] Core Research for Evolutional Science and Technology, Japan Science and Technology Agency, Saitama 332-0012, Japan. [4] Department of Immunology and Cell Biology, Graduate School of Medicine, WPI Immunology Frontier Research Center, Osaka University, Suita, Osaka 565-0871, Japan. [5] Department of Infection Metagenomics, Genome Information Research Center, Research Institute for Microbial Diseases, Osaka University, Suita, Osaka 565-0871, Japan. [6] Division of Mucosal Immunology, Department of Microbiology and Immunology, Institute of Medical Science, The University of Tokyo, Tokyo 108-8639, Japan. [7] Department of Microbiology, Kinki University Faculty of Medicine, Osaka-Sayama, Osaka 589-8511, Japan. [8] Laboratory of Lymphocyte Differentiation, WPI Immunology Frontier Research Center, Osaka University, Suita, Osaka 565-0871, Japan. [9] The Institute of Experimental Animal Sciences, Faculty of Medicine, Osaka University, Suita, Osaka 565-0871, Japan. [10] Laboratory for Mucosal Immunity, Center for Integrative Medical Sciences, RIKEN, Yokohama 230-0045, Japan. [11] Laboratory of Genomic Research on Pathogenic Bacteria, International Research Center for Infectious Diseases, Research Institute for Microbial Diseases, Osaka University, Suita, Osaka 565-0871, Japan. Correspondence and requests for materials should be addressed to K.T. (email: ktakeda@ongene.med.osaka-u.ac.jp).

Intestinal lamina propria plasma cells secrete IgA as a dimer, which is transported to the intestinal lumen by polymeric immunoglobulin receptor[1–4]. In the intestinal lumen, secretory IgA binds pathogens and pathogen-derived antigens to limit their invasion into the body[5,6]. In addition, secretory IgA contributes to the maintenance of gut homeostasis by regulating the activities and compositions of commensal bacteria[5,7–9]. Dysregulation of gut homeostasis caused by defective IgA responses can compromise host defenses against intestinal pathogenic bacteria and correlates with autoimmune diseases[10–12].

IgA-secreting cells develop in gut-associated lymphoid tissues (GALTs) such as Peyer's patches and solitary intestinal lymphoid tissues (SILTs) including cryptopatches, colonic patches and isolated lymphoid follicles (ILFs). Peyer's patches and ILF contribute to generation of IgA-secreting cells by different mechanisms[2,13,14]. However, it still remains unclear where and how IgA acquires antigen specificities and diversities. So far, characterization of IgA has focused on plasma cells residing in the small intestine. It has recently been reported that IgAs derived from the small and large intestines have differential repertoires[15]. It has also been reported that CCR9 mediates migration of IgA-secreting cells to the small intestine but not the large intestine[16], whereas CCR10 is involved in migration to both the small and large intestines[17]. However, it remains unclear where IgA-secreting plasma cells that migrate to the large intestine are generated.

In the appendix, a blind-ended tract linking the caecum, are lymphoid clusters called caecal patches. Compared with human caecal patches, which are present as multiple small clusters, mice possess a single large lymphoid cluster in the appendix[18]. As with Peyer's patches, caecal patches are covered by a monolayer of epithelial cells, among which M cells are present. Antigen-specific immunoglobulin responses and immunoglobulin diversification have been reported to occur in the appendix of rabbits[19,20]. Contrary to the above-mentioned evidences indicating that caecal patches are related to Peyer's patches, electron microscopy analysis has indicated that M cells on caecal patches have differential morphology to those on Peyer's patches[21]. Furthermore, it has been reported that appendectomy ameliorates intestinal inflammation observed in *Tcra*$^{-/-}$ mice or dextran sodium sulphate-treated mice[18,22]. Thus, caecal patches in the appendix are thought to possess unique functions compared with other GALTs. However, the roles of caecal patches in mucosal immune responses remain unclear.

In this study, we analysed the function of the mouse caecal patch using germ-free mice, in which intestinal IgA-secreting cells are severely decreased because of the absence of commensal bacteria. Surgical resection of the appendix results in slower accumulation of IgA-secreting cells in the large intestine, but not the small intestine, after conventionalization of germ-free mice. IgA$^+$ cells in the caecal patch migrate to both the large and small intestines, whereas those in Peyer's patches are preferentially recruited to the small intestine. IgA$^+$ cells generated in the caecal patch express increased levels of CCR10 compared with cells in Peyer's patches. Decreased number of colonic IgA-secreting cells correlates with altered composition of faecal microbiota in appendectomized mice at the early time point after colonization. These findings suggest that the caecal patch is a major site for the generation of IgA-secreting cells that migrate to the large intestine.

Results

Similar characteristics of caecal patches and Peyer's patches. There exists a single lymphoid cell cluster in the appendix of mice called caecal patch[18] (Fig. 1a). We compared immunological aspects of the characteristics of the caecal patch and Peyer's patches by immunohistochemistry (Fig. 1b). The caecal patch showed similar patterns of expression of CD4, B220 and CD11c to Peyer's patches, which are composed of B-cell-rich follicles, T-cell-rich parafollicular areas and a CD11c$^+$ cell-rich sub-epithelial dome region. Flow cytometry analysis indicated that the caecal patch and Peyer's patches contained similar numbers of IgM$^+$ B cells, IgA$^+$ B cells, CD4$^+$ cells and CD11c$^+$ cells (Fig. 1c, Supplementary Fig. 1). In addition, mRNA expression of genes encoding APRIL, BAFF and AID, which are involved in the class switching of immunoglobulin, in the caecal patch was equivalent to that observed in Peyer's patches and mesenteric lymph nodes (Fig. 1d). Peyer's patches in germ-free mice have been reported to be small[23]. Similarly, the size of the caecal patch in germ-free mice was reduced compared with specific-pathogen-free mice, indicating that the development of the caecal patch is dependent on commensal microbiota (Fig. 1e). Organogenesis of Peyer's patches has been reported to be initiated by the interaction of haematopoietic Rorγt$^+$ lymphoid tissue inducer (LTi) cells and stromal cells, which receive lymphotoxin signalling from LTi cells via lymphotoxin β receptor (LTβR). Mice lacking Rorγt(*Rorc(gt)*$^{gfp/gfp}$ mice) showed impaired development of LTi cells, and accordingly lacked Peyer's patches[24]. *aly/aly* mice that had a mutated gene encoding NF-κB-inducing kinase (NIK), which mediates LTβR signalling, showed impaired development of Peyer's patches[25]. These mutant mice also showed impaired caecal patch development (Fig. 1f). As previously reported, Peyer's patch cells from T-cell-deficient (*Tcrb*$^{-/-}$ *Tcrd*$^{-/-}$) mice produced lower, but substantial, amounts of IgA than those of the wild-type mice[26–28] (Fig. 1g). IgA production from caecal patch cells of *Tcrb*$^{-/-}$ *Tcrd*$^{-/-}$ mice was also similarly reduced, thus indicating that

Figure 1 | Similar immunological characteristics of the caecal patch and Peyer's patches. (**a**) Haematoxylin and eosin staining of the caecal patch (CP) in the appendix and Peyer's patches (PP) in the small intestine of specific-pathogen-free mice. Scale bars, 100 μm. (**b**) Distribution of immune cells in CP and PP. Frozen sections were stained for B220 (green), CD4 (red), CD11c (grey) and DAPI (blue), and analysed by confocal fluorescence microscopy. Scale bars, 100 μm. (**c**) B-cell populations in CP and PP of specific-pathogen-free (SPF) mice. Cells were stained with anti-IgA, IgM and B220 mAbs, and analysed by flow cytometry. Numbers within dot plots indicate percentages of cells in respective areas. (**d**) Expression of immunoglobulin class switching-related genes. Expression of mRNA for *Tnfsf13* (encoding APRIL), *Tnfsf13c* (encoding BAFF) and *Aicda* (encoding AID) in PP, CP and mesenteric lymph node (MLN) were quantitatively analysed by real-time RT-PCR, and normalized to that of *Gapdh*. Data represent mean ± s.d. ($n=4$ per group), and representations of two independent experiments are shown. (**e**) Development of the caecal patch in SPF or germ-free (GF) mice. Left: gross appearance of the appendix. The caecal patch was visualized based on a B220$^+$ cluster of whole-mount staining. Middle and right: haematoxylin and eosin staining of the appendix. The boxed areas in the middle panels are enlarged on the right. Scale bars, 1 mm (left), 300 μm (middle) and 100 μm (right). (**f**) Development of the caecal patch in *Rorc(gt)*$^{gfp/+}$ or *Rorc(gt)*$^{gfp/gfp}$ mice (upper) and WT or *aly/aly* mice (lower). Arrows indicate CP (**e**,**f**). Original magnification, ×7 (left panels in **e** and **f**). Scale bars, 1 mm. (**g**) IgA production by mononuclear cells from PP and CP. Mononuclear cells from PP and CP of WT and *Tcrb*$^{-/-}$ *Tcrd*$^{-/-}$ mice were cultured for 3 days and the supernatant was analysed by ELISA. Data represent mean ± s.d. of triplicate samples in one experiment, and representations of two independent experiments are shown. Statistical analyses were performed with the Student's *t*-test. *$P<0.05$.

the caecal patch as well as Peyer's patches mediate both T cell-dependent and -independent IgA inductions. Thus, the caecal patch and Peyer's patches show analogous features of immunological structures, function and developmental processes.

Delayed colonic IgA$^+$ cell recruitment without caecal patch. Given that the caecal patch showed similar properties to Peyer's patches, which are typical GALTs mediating immune responses, we investigated the immunological function of the caecal patch by generating caecal patch-deficient mice. To assess the effect of caecal patch deficiency on the development of intestinal immunity, we utilized germ-free mice, which showed normal development of the adaptive immune system after bacterial colonization in the gut. We removed the appendix of germ-free mice by surgery, and then transferred and reared them in a conventionalized (specific-pathogen-free) environment (Supplementary Fig. 2). At 4 weeks after conventionalization,

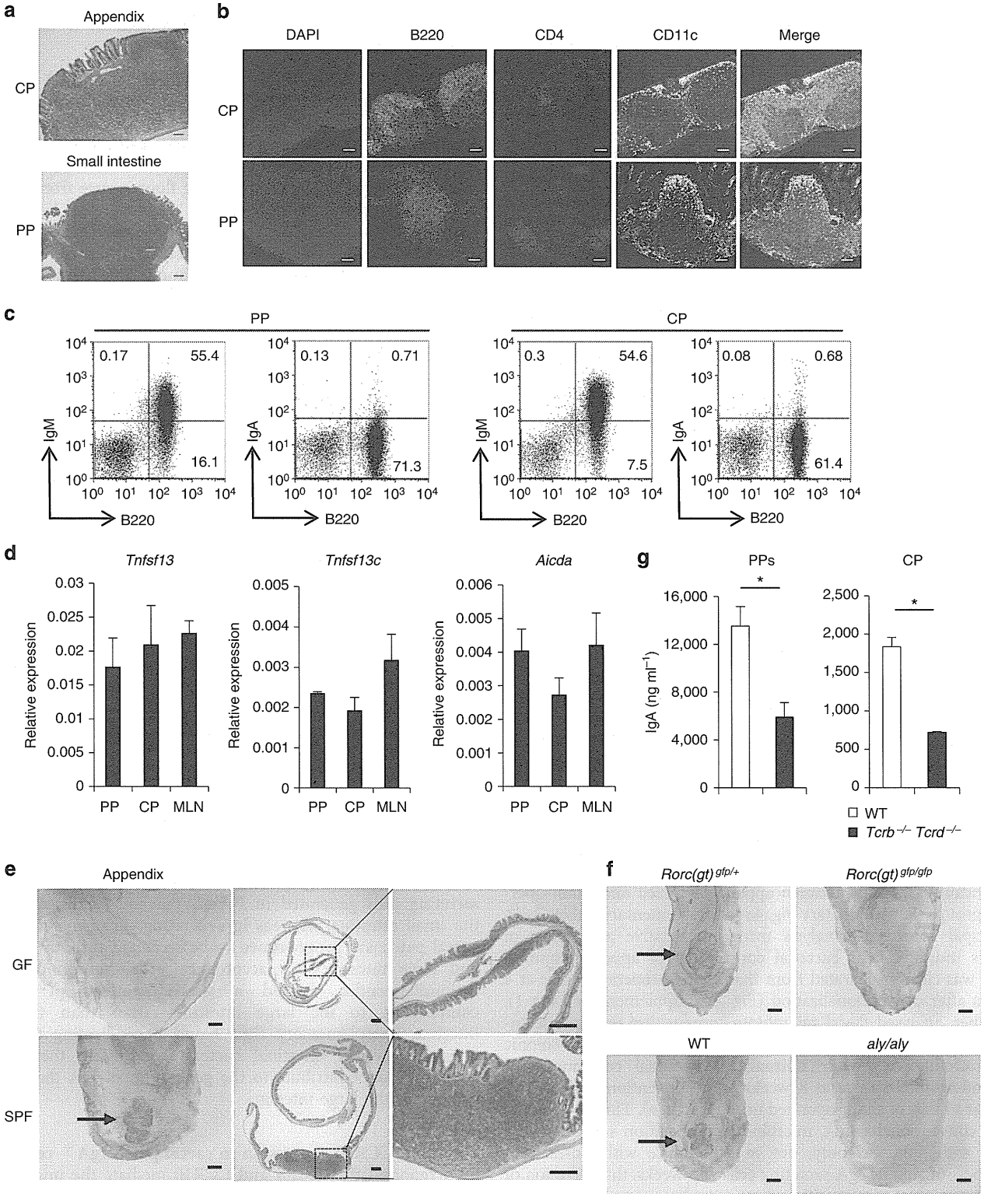

mice were analysed for the number of IFN-γ-, IL-17- and IL-10-producing $CD4^+$ T cells and IgA^+ cells in the small and large intestines (Fig. 2a,b and Supplementary Fig. 3). IFN-γ-, IL-17- and IL-10-producing $CD4^+$ T cells all increased in numbers similarly in the small and large intestines of sham-operated and appendectomized mice. IgA^+ cells in the small intestine of sham-operated and appendectomized mice also increased to a similar extent after conventionalization. However, the number of IgA^+ cells in the large intestine markedly decreased in appendectomized mice compared with sham-operated mice. The decrease in number of IgA^+ cells in large intestinal lamina propria was further confirmed by immunohistochemical analysis (Fig. 2c). IgA^+ cells were scarcely observed in germ-free mice, and conventionalization of sham-operated germ-free mice increased the number of IgA^+ cells. In contrast, the number of IgA^+ cells in large intestinal lamina propria did not dramatically increase after conventionalization of germ-free mice with the appendectomy at 4 weeks after conventionalization. We next analysed concentration of secretory IgA in faeces and serum at 4 weeks after conventionalization (Fig. 2d). Levels of secretory IgA in faeces, but not in serum, in appendectomized mice were lower than those in sham-operated mice. Thus, accumulation of IgA-secreting cells selectively decreased in the large intestine of appendectomized mice at 4 weeks after conventionalization. We then analysed time-dependent increase of IgA^+ cells in the large intestine by measuring IgA^+ cell number at 2, 4 and 8 weeks after conventionalization (Fig. 3a–c). At 2 weeks as well as 4 weeks, the number of IgA^+ cells was markedly decreased in appendectomized mice. However, at 8 weeks, the number of IgA^+ cells of appendectomized mice was comparable to that of sham-operated mice. Taken together, these findings indicate that accumulation of IgA-secreting cells to the large intestine was delayed in mice with appendectomy.

Altered faecal microbiota composition in appendectomized mice. As secretory IgA is responsible for the control of intestinal bacteria, we analysed the composition of faecal microbiota in appendectomized and sham-operated mice at 4 weeks after conventionalization by pyrosequence-based 16S rRNA gene profiling. The rarefaction curve showed that the estimated operational taxonomic units (OTUs) of appendectomized mice were less abundant than those of sham-operated mice and that the sufficient sequencing depth has been achieved in both groups (Fig. 4a). In the class distribution, the relative abundance of several bacterial groups such as *Bacilli*, *Erysipelotrichi* and *Gammaproteobacteria* in appendectomized mice was higher than that in sham-operated mice; *Mollicutes*, *Deferribacteres*, *Betaproteobacteria* and *Deltaproteobacteria* were less abundant in appendectomized mice (Fig. 4b, Supplementary Table 1). Analyses at the other levels also showed that the relative abundance of many bacterial groups was significantly different between appendectomized and sham-operated groups (Supplementary Fig. 4a–c, Supplementary Tables 2–4). Principal coordinate analysis using the relative abundance of OTUs indicated that bacterial community of appendectomized mice was clearly separated from that of sham-operated mice at 4 weeks after conventionalization (Fig. 4c, Supplementary Data 1). We then analysed faecal microbiota composition in appendectomized mice at 8 weeks after conventionalization when colonic IgA-secreting cells were normalized. Bacterial community of appendectomized mice at 8 weeks after conventionalization was similar to that of sham-operated mice (Fig. 4d,e). Thus, at 4 weeks after conventionalization, microbiota composition was altered in mice with appendectomy, but in accordance with normalized numbers of colonic IgA-secreting cells at 8 weeks, the alteration of faecal microbiota composition disappeared.

To exclude the possibility that the incision of the appendix itself caused the slow accumulation of IgA-secreting cells and the altered composition of microbiota in the large intestine, we cut and sutured the appendix without excision, and analysed the number of IgA-secreting cells and faecal microbiota at 4 weeks after conventionalization (Supplementary Fig. 5a–d). In these enterotomized mice, no alteration of the IgA-secreting cells and microbiota composition was observed compared with sham-operated mice, which underwent incision of the abdomen alone. Thus, appendectomized mice, which showed delayed accumulation of IgA^+ cells in the large intestine, had altered configurations of faecal microbiota at 4 weeks after conventionalization.

Recruitment of caecal patch IgA^+ cells to the colon. We analysed the mechanisms for the slower increase of colonic IgA-secreting cells in appendectomized mice using Kaede-transgenic mice, in which *in vivo* cell migration can be monitored[29]. Kaede is a photoconvertible protein, changing fluorescence from green to red with exposure of violet light. We generated Kaede bone marrow chimeric mice, in which bone marrow cells were reconstituted with those of Kaede-transgenic mice. The caecal patch from Kaede bone marrow chimeric mice was exposed to violet light for 5 min to induce photoconversion of Kaede proteins expressed in haematopoietic cell types present in this region. After exposure, 93.8 ± 3.2% of cells isolated from caecal patches expressed a red fluorescence signal (Kaede-red) (Supplementary Fig. 6). At 3 and 7 days after photoconversion, the number of Kaede-red cells gradually decreased in the caecal patch (Fig. 5a). Accordingly, Kaede-red IgA^+B220^- cells increased similarly in the lamina propria of the small and large intestines at the 7-day time point (Fig. 5b). We also exposed Peyer's patches to violet light, and analysed migration of Peyer's patch-derived IgA^+ cells to intestinal lamina propria. Kaede-red IgA^+B220^- cells were observed both in the small and large intestines at 7 days after photoconversion. However, the percentage of Kaede-red IgA^+ cells in total IgA^+ cells was markedly reduced in the large intestine compared with the small intestine (Fig. 5c). These findings indicate that IgA-secreting cells generated in the caecal patch migrate to both the small and large intestines, but IgA-secreting cells generated in Peyer's patches preferentially migrate to the small intestine. To corroborate these findings, we transferred $CD45.2^+$ $B220^+$ cells from caecal patches and Peyer's patches into $CD45.1^+$ mice. At 7 days after transfer, $CD45.2^+IgA^+$ cells in the small and large intestines of $CD45.1^+$ mice were measured (Fig. 5d). Similarly to the results obtained from experiments using Kaede bone marrow chimeric mice, IgA^+ cells isolated from caecal patches migrated to both the small and large intestines. In contrast, IgA^+ cells isolated from Peyer's patches were preferentially recruited to the small intestine. Taken together, these findings suggest that IgA-secreting cells generated in Peyer's patches mainly migrate to the small intestine, whereas IgA-secreting cells generated in the caecal patch are programmed to be recruited to both the small and large intestines. In accordance with these findings, the caecum/appendix showed a similar pattern of bacterial composition to the large intestine rather than the small intestine (Supplementary Figs 7 and 8), indicating that large intestine-types of intestinal bacteria residing in the caecum/appendix may contribute to the generation of IgA that acts on bacteria of the large intestine.

Enhanced CCR10 expression in caecal patch IgA^+ cells. It has been reported that CCR9 and CCR10 mediate the migration of IgA^+ cells to the intestinal lamina propria[30]. Therefore, we used

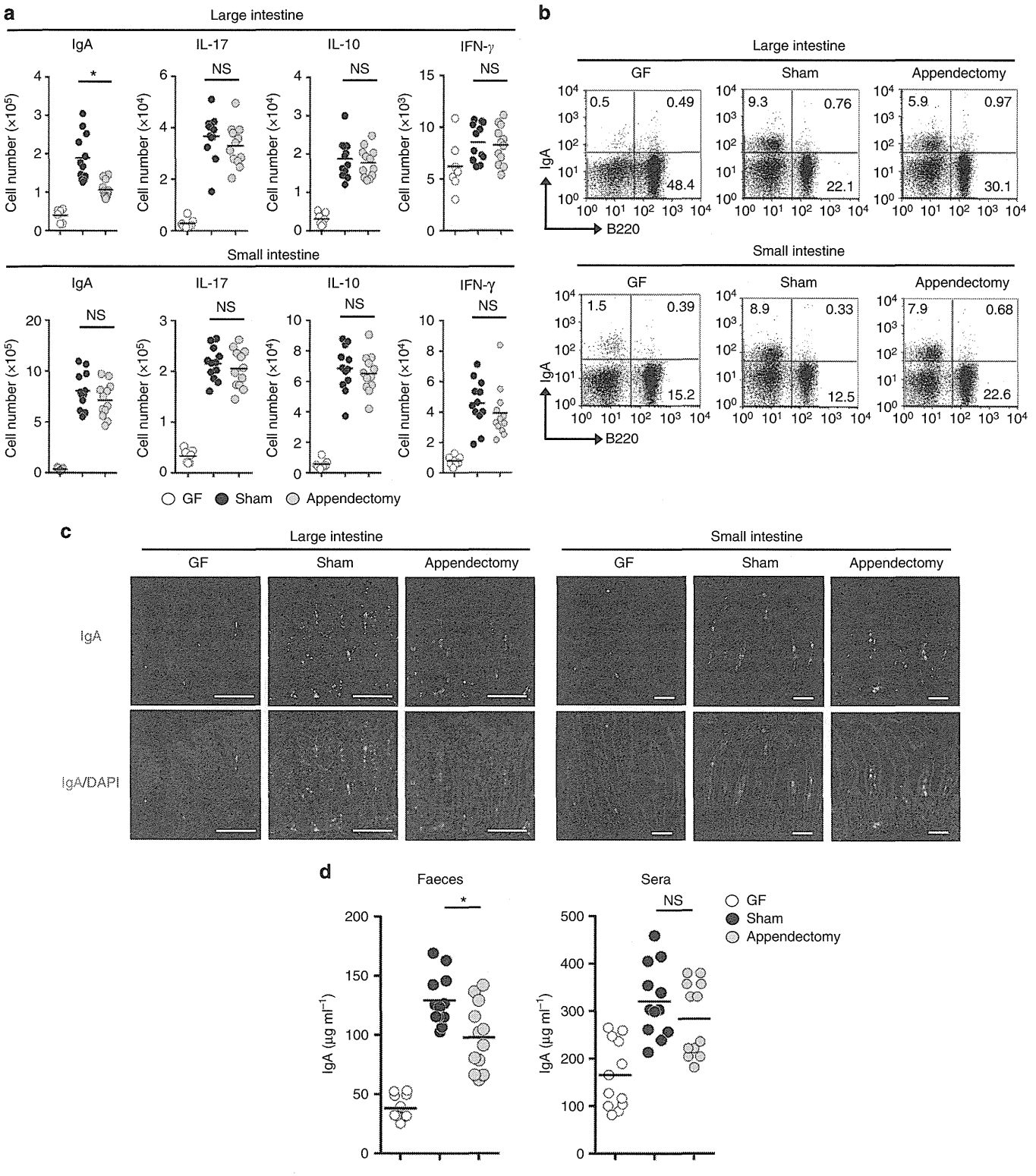

Figure 2 | Decreased IgA-secreting cells in large intestinal lamina propria of appendectomized germ-free mice after conventionalization. (**a**,**b**) Lamina propria lymphocytes were isolated from appendectomized or sham-operated germ-free(GF) mice at 4 weeks after conventionalization, and stained for surface IgA/B220 or intracellular IL-17/IFN-γ/IL-10 in $CD4^+$ population. (**a**) Total numbers of IgA^+ $B220^-$ cells as well as IL-17-, IFN-γ- and IL-10-positive $CD4^+$ cells in the large (upper) and the small intestine (lower) are shown. Each symbol represents an individual mouse, and horizontal bars indicate the mean. (**b**) Representative dot plots for cells stained with anti-IgA and B220 of appendectomized and sham-operated mice. Numbers within plots indicate percentages of cells in respective areas. (**c**) Distribution of IgA^+ cells in the small and large intestines. Frozen sections were stained with anti-IgA mAb (green) and DAPI (blue). Scale bars, 100 μm. (**d**) Faeces and sera were collected from appendectomized ($n=12$) or sham-operated mice ($n=12$) at 4 weeks after conventionalization and GF mice ($n=12$), and IgA levels of faeces and sera were determined by ELISA. Each symbol represents an individual mouse, and horizontal bars indicate the mean. Statistical analyses were performed with the Student's *t*-test. *$P<0.05$. NS, not significant.

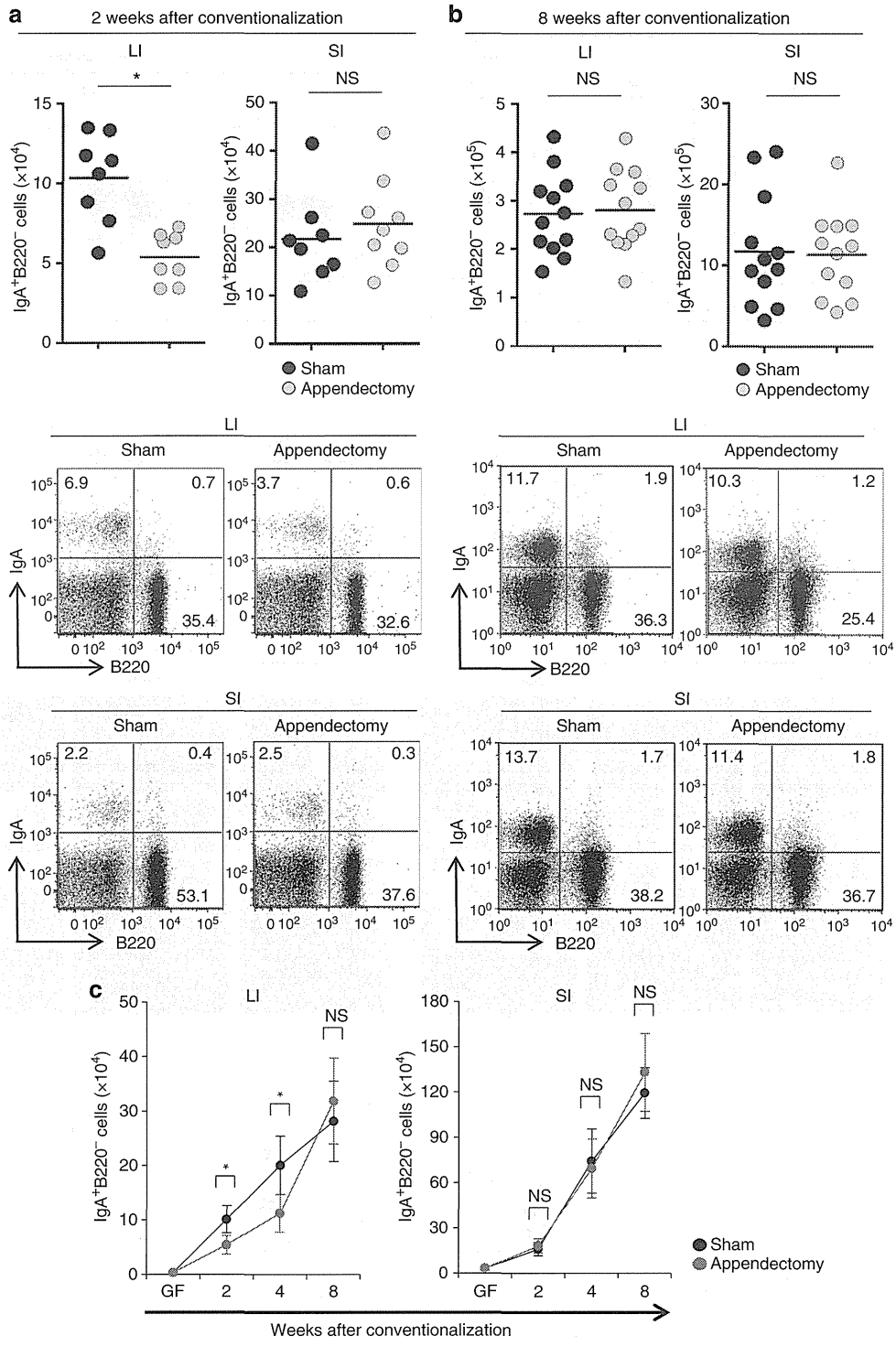

Figure 3 | The number of IgA-secreting cells in the large intestine at 2 and 8 weeks after conventionalization. (**a**,**b**) Lamina propria lymphocytes were prepared from appendectomized or sham-operated mice at 2 weeks (**a**) and 8 weeks (**b**) after conventionalization, and analysed for the expression of surface IgA and B220 by flow cytometry. Total numbers of IgA$^+$ B220$^-$ cells in the small or large intestines are shown. Each symbol represents an individual mouse, and horizontal bars indicate the mean. Representative dot plots of intestinal leukocytes prepared from appendectomized and sham-operated mice are shown. Numbers within plots indicate percentages of cells in respective areas. (**c**) The numbers of IgA$^+$ B220$^-$ cells in the small and large intestines of appendectomized and sham-operated mice at indicated time points after conventionalization. The experiments were performed more than two times with similar results. Data represent mean ± s.d. (four mice per group). SI, small intestine; LI, large intestine. Statistical analyses were performed with the Student's *t*-test. *$P<0.05$. NS: not significant.

anti-CCR9 mAb and CCL27-Fc chimera protein to analyse surface expression of CCR9 and CCR10 on IgA$^+$ cells, which were positive for the plasmablast marker CD138 (Supplementary Fig. 9), in the caecal patch and Peyer's patch (Fig. 6a,b). CCR9 was similarly expressed on IgA$^+$ cells in the caecal patch and Peyer's patch. In contrast, expression of CCR10 determined by

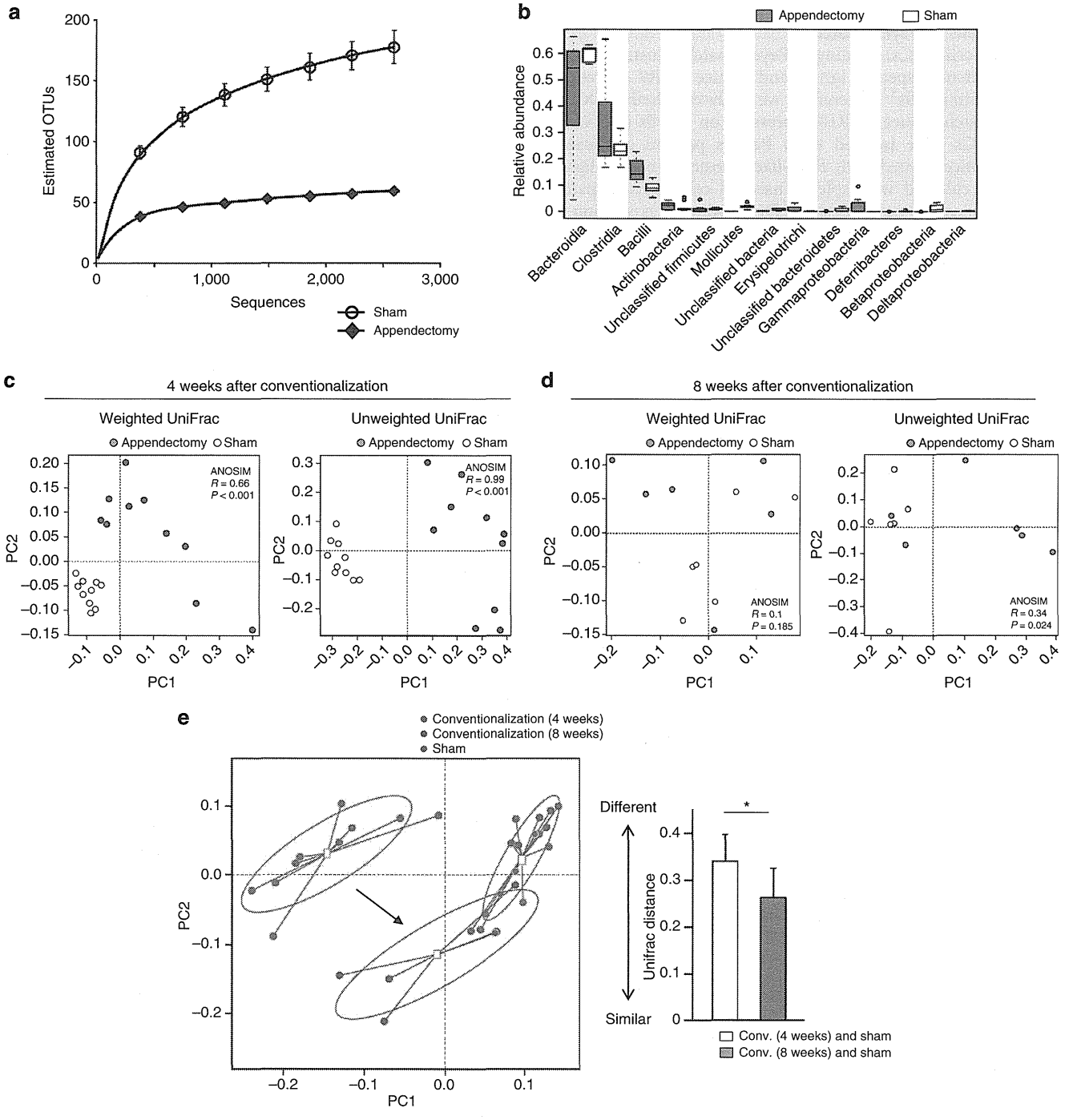

Figure 4 | Altered composition of faecal microbiota in appendectomized mice. Faecal microbiota in mice with appendectomy ($n=10$) and sham-surgery ($n=10$) at 4 weeks and 8 weeks after conventionalization was analysed by pyrosequence-based 16S rRNA gene profiling. (**a**) Rarefaction curves of sham-operated and appendectomized groups at 4 weeks after conventionalization. The vertical axis shows the number of observed species that would be expected to be found after sampling the number of sequences shown on the horizontal axis. The number of taxa was at a 3% dissimilarity level. Data represent mean ± s.d. (**b**) A box plot of class level-bacterial composition of appendectomized and sham-operated mice at 4 weeks after conventionalization. The box for each group represents the interquartile range (25–75th percentile) and the line within the box is the median value. The bottom and top bars indicate the 10th and 90th percentile, respectively. Open circles represent outlier values. The results of statistical test were described in Supplementary Table 1. (**c**,**d**) The principal coordinate analysis (PCoA) using OTUs based on the weighted (left) and unweighted (right) UniFrac distances. Faecal microbiota of appendectomized mice at 4 weeks (**c**) or 8 weeks (**d**) after conventionalization was compared with that of sham-operated mice. For statistical analysis, ANOSIM was calculated using R package 'Vegan'. (**e**) PCoA of faecal microbiota in mice with appendectomy and sham-surgery at 4 weeks and 8 weeks after conventionalization using OTUs (left). Red, blue and green circles indicate the clusters of mice with appendectomy at 4 weeks, 8 weeks after conventionalization and sham-operated mice, respectively. The UniFrac distance is calculated between pairs of samples (right). Statistical analyses were performed with the Student's *t*-test. *$P<0.05$.

CCL27-binding in caecal patch IgA$^+$ cells was markedly higher than IgA$^+$ cells in Peyer's patches.

Dendritic cells (DCs) residing in Peyer's patches instruct B cells to secrete microbe-specific IgA[31], and induce CCR9 expression on IgA-secreting cells[32]. Therefore, we analysed whether DCs in the caecal patch induce CCR10 expression on B cells (Fig. 6c,d). CD11c$^+$ DCs were isolated from Peyer's patches and caecal patches of mice treated with FMS-like tyrosine kinase 3 ligand (Flt3L) and cultured with splenic naive B cells. Peyer's patch-derived and caecal patch-derived DCs induced expression of CCR9 on B cells. In contrast, Peyer's patch-derived DCs failed to induce CCR10 expression on cocultured B cells. However, B cells cocultured with caecal patch-derived DCs expressed increased levels of CCR10. Thus, DCs residing in the caecal patch were able to induce CCR10 expression.

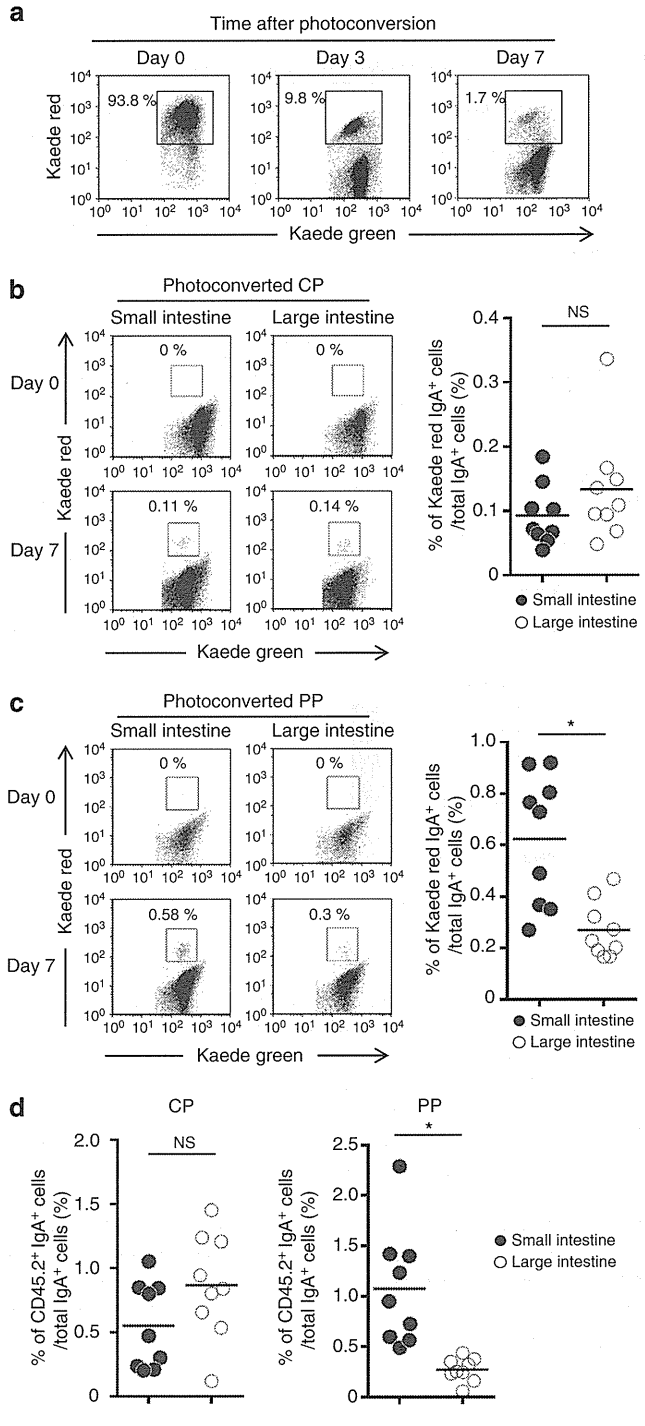

Figure 5 | Recruitment of caecal patch, but not Peyer's patch, IgA-secreting cells to the colon. (**a**) The caecal patch in the appendix from Kaede bone marrow chimeric mice were exposed to violet light for 5 min and resected immediately (day 0), or 3 and 7 days after violet light exposure. Cells from photoconverted caecal patches were subjected to flow cytometry at indicated time points to evaluate photoconversion. Numbers within plots indicate percentages of cells in respective areas. Data are representative of three independent experiments. (**b**,**c**) The caecal patch (CP) (**b**) or Peyer's patches (PP) (**c**) were exposed to violet light for 5 min, and the percentages of Kaede-red IgA$^+$ cells in total IgA$^+$ cells in the intestines were analysed at 7 days after photoconversion. Representative dot plots of cells in the intestinal lamina propria are shown (left). Right panel shows the percentages of photoconverted IgA$^+$cells in total IgA$^+$cells of intestinal lamina propria. Each symbol represents an individual mouse, and horizontal bars indicate the mean. (**d**) B220$^+$cells from CD45.2 mice were transferred into CD45.1 C57BL/6 recipient mice. CD45.2$^+$IgA$^+$cells in intestinal lamina propria from CD45.1 C57BL/6 mice were analysed at 7 days after cell transfer. Data show the percentages of CD45.2$^+$ IgA$^+$ cells in total IgA$^+$cells of intestinal lamina propria. Each symbol represents an individual mouse, and horizontal bars indicate the mean. Statistical analyses were performed with the Student's *t*-test. *$P<0.05$. NS, not significant.

Increased colonic lymphoid clusters without caecal patch. ILFs are sites of generation of IgA-secreting cells with differential mechanisms to those from Peyer's patches[26]. In the absence of CCR10, SILTs including ILFs have been reported to enlarge and increase in number, which contributed to the maintenance of a normal number of IgA-secreting cells in the intestine of *Ccr10*$^{-/-}$ mice[17]. Therefore, we measured the number of SILTs in the large intestine of appendectomized mice by whole-mount staining of B220$^+$ cells at 8 weeks after conventionalization (Fig. 7). The number of SILTs in the small intestine did not alter in appendectomized mice. In contrast, there were more SILTs in the large intestine of appendectomized mice than that of sham-operated mice. In addition, the size of each SILT was slightly larger in the large intestine of appendectomized mice. Thus, normalization of colonic IgA-secreting cells at 8 weeks correlates with the increased and enlarged SILTs.

Discussion

In this study, we show that in the absence of the caecal patch, the number of IgA-secreting cells in the large intestine increased with markedly delayed kinetics after bacterial colonization. Subsequent analyses demonstrated that IgA-secreting plasmablasts migrate to the large and small intestines from the caecal patch, but plasmablasts in Peyer's patches are mainly recruited to the small intestines. DCs in caecal patches, but not in Peyer's patches, effectively induced expression of CCR10, which mediates recruitment of plasmablasts to both the small and large intestines. In line with the decreased number of IgA-secreting cells in the large intestine of appendectomized mice, the composition of microbiota in faeces altered compared with that of sham-operated mice at 4 weeks after conventionalization.

We generated mice lacking the caecal patch using germ-free mice that developed normal adaptive immunity after colonization of microbiota. Appendectomy has been performed in mice reared in specific-pathogen-free condition[18,22]. However, in this condition, mice suffered from peritonitis due to extravasation of microbiota via surgical wound sites, and are therefore unsuitable for analysis of intestinal immune responses in the

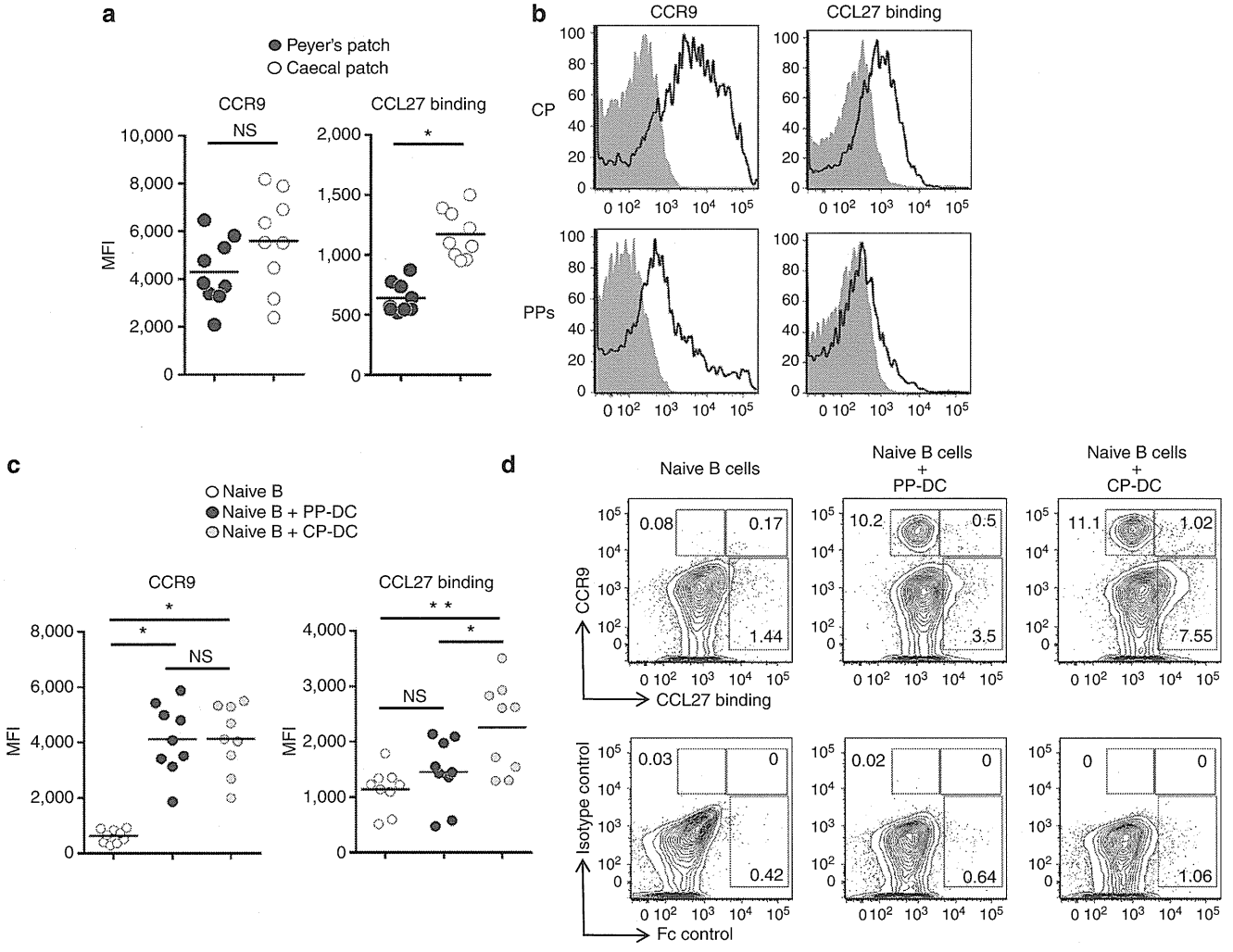

Figure 6 | Enhanced CCR10 expression in caecal patch IgA-producing cells. (**a**,**b**) Expression of CCR9 and CCR10 on IgA$^+$ cells in Peyer's patch and the caecal patch. IgA$^+$B220$^+$ cells prepared from Peyer's patches (PP) or caecal patch (CP) of specific-pathogen-free mice were analysed for expression of CCR9 and CCR10 using anti-CCR9 mAb and CCL27-Fc chimera protein, respectively. (**a**) The mean fluorescence intensity (MFI) of the indicated surface markers on PP or CP IgA$^+$cells is shown. Each symbol represents an individual mouse, and horizontal bars indicate the mean. (**b**) Histograms gated on IgA$^+$ B220$^+$ cells from PP or CP. Solid line: CCR9 expression or CCL27 binding, grey histogram: human IgG Fc or isotype control. (**c**,**d**) Induction of CCR9 and CCR10 on IgA$^+$ cells by GALT-DCs. CD11c$^+$ cells were isolated from PP and CP of mice injected with B16 melanoma cells secreting Flt3L. Splenic naive B cells were cultured in the presence of antibody to IgM alone or with CP-derived DCs (CP-DC) or PP-derived DCs (PP-DC). After 4 days, B cells were analysed for CCR9 expression and CCL27 binding. (**c**) Each symbol represents an individual mouse, and horizontal bars indicate the mean. (**d**) Representative dot blots gated on B220$^+$ cells are shown. Statistical analyses were performed with the Student's *t*-test. $^*P<0.05$. $^{**}P<0.005$, NS, not significant.

healthy state. In contrast, surgical operation of the appendix in germ-free mice did not cause inflammation because of an absence of microbiota, and the sutured wounds were almost completely closed within 1 week without any sign of inflammation. In addition, resection of the appendix did not cause dramatic reduction of the luminal space of the caecum as shown in Supplementary Fig. 2. This enabled us to investigate the development of mucosal immunity in appendectomized mice after conventionalization.

In accordance with the decreased number of IgA-secreting cells in the large intestine, the composition of faecal microbiota altered in appendectomized mice at 4 weeks after conventionalization. Therefore, as has been reported in the small intestine[7,8,12], generation of IgA-secreting cells appears responsible for the maintenance of microbial homeostasis in the large intestine. Intriguingly, appendectomized mice at the early time point after conventionalization showed diverse patterns of microbial communities between individuals, whereas sham-operated mice contained microbiota that were highly homogeneous to each other. Thus, colonic secretory IgA contributes to shaping the microbial patterns characteristic of mice.

IgAs in the small and large intestines have been reported to possess differential repertoires[15]. The differential diversities are thought to occur before plasma cell recruitment to the small and large intestines[15]. However, the events that govern the generation of distinct specificities of IgA remain unknown. The present study provides evidence that the caecal patch is the major site for the generation of plasmablasts migrating to both the small and large intestines, whereas Peyer's patches are areas that generate plasmablasts that show preferential migration to the small intestine. Secretory IgA, which has differential diversities between the small and large intestines, has been shown to control gut microbiota[5,7–9,12]. As has been reported in the human intestine[33], the caecum showed a similar pattern of bacterial

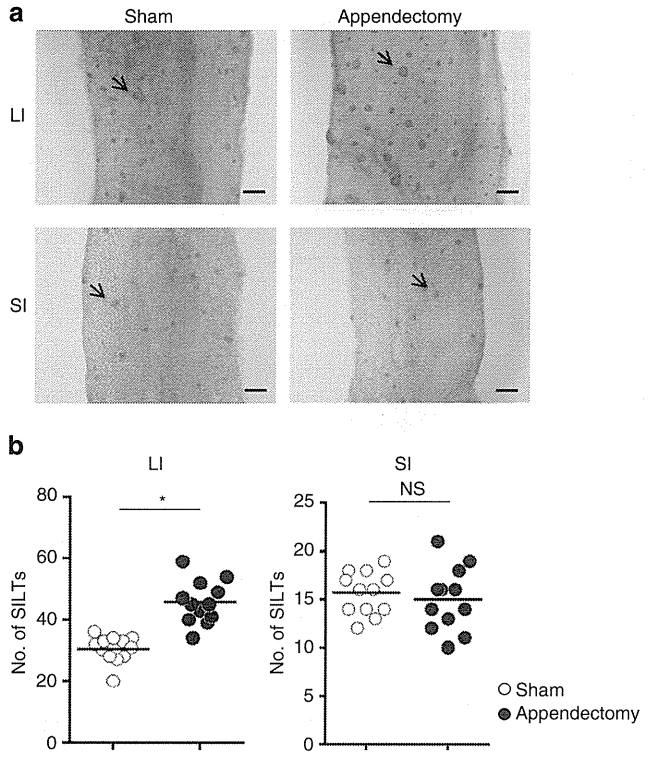

Figure 7 | Increased numbers of isolated lymphoid clusters in the colon of appendectomized mice. (**a**) SILTs were visualized based on B220$^+$ clusters (arrows) of whole-mount staining of intestines. Representative photos are shown. (**b**) Numbers of SILTs per surface of intestines (in a 25 mm square) are shown (12 mice analysed). Each symbol represents an individual mouse, and horizontal bars indicate the mean. Original magnification: ×7. Scale bars, 1 mm. SI: small intestine, LI: large intestine. Statistical analyses were performed with the Student's *t*-test. *$P<0.05$. NS, not significant.

composition to the large intestine. Thus, it is supposed that IgA generated in the caecal patch, which is exposed to the large intestine-types of microbiota, controls microbiota composition in the large intestine. However, at 8 weeks after conventionalization, microbiota composition was normalized in the large intestine of mice with appendectomy. Therefore, IgA generated in lymphoid tissues other than the caecal patch also contributes to the maintenance of microbiota homeostasis. Indeed, colonic SILTs including ILFs increased in mice with appendectomy.

The chemokine receptors CCR9 and CCR10 have been shown to mediate the migration of IgA-secreting plasmablasts to the intestine. CCR9 is responsible for the homing to the small intestine[16], whereas CCR10 contributes to the migration to both the small and large intestines[17,34,35]. IgA$^+$ cells in the caecal patch expressed higher levels of CCR9 and CCR10 than the cells in Peyer's patches. Therefore, the higher expression of CCR10 on IgA-secreting cells generated in the caecal patch might be responsible for the preferential migration to the large intestine compared with cells instructed in Peyer's patches. In accordance with the finding that DCs residing in Peyer's patches induce generation of IgA-secreting cells and expression of CCR9 (ref. 32), DCs residing in the caecal patch induced enhanced levels of CCR10. Thus, IgA-secreting cells generated in the caecal patch might be programmed to migrate to the large intestine with enhanced CCR10 expression. CD11c$^+$ DCs residing in Peyer's patch and the caecal patch showed differential activity in terms of CCR10 induction on IgA$^+$ cells. It would be an interesting future study to analyse the mechanisms of the differential properties of DCs residing in Peyer's patch and the caecal patch.

In contrast to the decreased number of IgA-secreting cells observed in the large intestine of appendectomized mice, the number of CD4$^+$ T cells producing IFN-γ, IL-17 or IL-10 in the small and large intestines did not change. In this regard, several unique subsets of intestinal DCs that instruct development of Th1, Th17 or regulatory T cells have been identified[36]. These DCs reside in the lamina propria to sample luminal antigens, and migrate to mesenteric lymph nodes, where they induce effector and regulatory CD4$^+$ T cells[37–39]. Thus, unlike IgA-secreting cells, development of helper and regulatory T cells are mediated by DCs that reside in the lamina propria. Therefore, the absence of the caecal patch did not affect T-cell development in the intestine.

ILF has been shown to contribute to T-cell-independent IgA synthesis, the mechanism of which is different from that observed in Peyer's patches[26]. In addition, ILFs have been shown to increase in number in the small and large intestines of mice lacking CCR10, which show normal numbers of IgA-secreting cells in the intestine[17]. Enlarged ILFs are considered to serve to compensate for the defective recruitment of *Ccr10*$^{-/-}$ IgA-secreting cells to the intestine. Similarly to *Ccr10*$^{-/-}$ mice, the number and size of ILFs in the large intestine increased in appendectomized mice in the current study. However, unlike *Ccr10*$^{-/-}$ mice, which showed increased and enlarged SILTs in the small intestine, SILTs did not increase in the small intestine of mice with appendectomy after bacterial colonization. In this regard, CCR10$^+$ IgA$^+$ cells generated in the colonic SILTs might be able to migrate to both the small and large intestine in our study. However, in the absence of CCR10, IgA$^+$ cells generated in the enlarged colonic SILTs were impaired in the migration to the small intestine and therefore SILTs in the small intestine might be enlarged in *Ccr10*$^{-/-}$ mice.

Collectively, our results demonstrate that a lymphoid organ in the appendix is a major tissue generating IgA$^+$ cells migrating to the large intestine. Peyer's patches and the caecal patch have distinct properties in terms of induction of IgA$^+$ cells with differential migratory directions. This might correlate with the distinct functions of secretory IgAs in the small and large intestines. The precise characterization of IgA generated in Peyer's patches and the caecal patch will reveal how differential IgA repertoires between the small and large intestines are generated in the future.

Methods

Mice. C57BL/6J mice and CD45.1 congenic mice of the C57BL/6 background (6–8-week old) were purchased from Japan SLC and Sankyo Laboratories Japan, respectively. ALY/NscJcl-*aly* (*aly/aly*) and ICR mice were from CLEA Japan. Kaede-transgenic mice[29] were kindly provided by Dr Michio Tomura (Kyoto University). These mice were kept under specific-pathogen-free conditions at the Experimental Animal Facility, Graduate School of Medicine, Osaka University. Germ-free (IQI/Jic[Gf] ICR) mice were from CLEA Japan and maintained under germ-free conditions. *Tcrb*$^{-/-}$*Tcrd*$^{-/-}$ (refs 40,41) and *Rorc(gt)*$^{gfp/gfp}$ mice[42] of the C57BL/6 background were from Jackson Laboratory, and maintained at the Experimental Animal Facility, Institute of Medical Science, The University of Tokyo. Both male and female mice were used for the all experiments. All animal experiments were performed in accordance with the guidelines of Osaka University Animal Experiment and the Animal Care and Use Committee, The University of Tokyo.

Antibodies. FITC anti-IgM (1B4B1) and Phycoerythrin (PE) anti-IgA (11-44-2) mAbs were purchased from Southern Biotech. Pacific Blue anti-CD45R/B220 (RA3-6B2), FITC anti-CD45R/B220 (RA3-6B2), unlabelled anti-CD16/32 (2.4G2), biotin anti-IgA (C10-1), FITC anti-IgA (C10-3), APC rat IgG$_{2a}$ isotype, APC anti-CD138/Syndecan-1 (281-2) and PE anti-CD11c (HL3) mAbs were from BD Biosciences. PerCP/Cy5.5 anti-CD4 (GK1.5), PE anti-IL-10 (JES5-16E3), Alexa Fluor 647 anti-IL-17A (TC11-18H10.1), FITC anti-IFN-γ (XMG1.2), APC/Cy7 anti-CD45R/B220 (RA3-6B2), Pacific Blue anti-CD45.2 (clone 104), Pacific Blue

anti-CD11b (M1/70), Alexa Fluor 647 anti-mouse CCR9 (CW-1.2) mAbs and Alexa Fluor 647 mouse IgG_{2a} were from Biolegend. Human CCL27-Fc and control-Fc chimera proteins were as described previously[34]. Briefly, 293T cells were transfected with the CCL27-Fc and control-Fc expression vectors using Lipofectamine 2000 (Invitrogen). The culture supernatants containing these chimera proteins were collected and used for the experiments.

Quantitative real-time PCR. Total RNA was extracted with TRIzol reagent (Life Technologies). After treated with RQ1 DNase I (Promega), total RNA was reverse transcribed using M-MLV reverse transcriptase (Promega) and random primers (Toyobo). Complementary DNA was analysed by qPCR using GoTaq qPCR Master Mix (Promega) and an ABI 7300 system (Applied Biosystems). All values were normalized against the amount of glyceraldhyde-3-phosphate dehydrogenase (GAPDH) in each sample. Amplification conditions were: 50 °C (2 min), 95 °C (10 min) and 40 cycles of 95 °C (15 s) and 60 °C (60 s). The following primer sets were used:*Gapdh*, 5′-CCTCGTCCCGTAGACAAAATG-3′ and 5′-TCTCCACTT TGCCACTGCAA-3′; *Tnfsf13*, 5′-AGACATTGTACGAGTCTGGGA-3′ and 5′-TCCCTTGTCCTTCCCGAGATA-3′; *Tnfsf13c* 5′-ATAGTGGTGAGGCAAAC AGGC-3′ and 5′-CGTCCCCAAAGACGTGTACTT-3′; *Aicda*, 5′-AACCAGACA ACTTCGGCGCAT-3′ and 5′-TCATCACGTGTGACATTCCAG-3′.

Immunohistological staining. Collected tissues were fixed with 4% paraformaldehyde for 1 h at 4 °C. After washing, tissues were incubated in a 30% sucrose solution overnight at 4 °C, and embedded in OCT compound (Sakura Finetech). Frozen sections of lymphoid tissues (10 μm) were blocked with PBS containing 0.5% Triton X-100 (PBS-T) and 3% bovine serum albumin (BSA), and incubated with APC anti-CD11c (5 μg ml^{-1}), FITC anti-CD45R/B220(5 μg ml^{-1}) and biotin anti-CD4 mAbs (5 μg ml^{-1}), followed by streptavidin-Alexa Fluor 568 (Life Technologies) (2 μg ml^{-1}). Alternatively, frozen sections were incubated with FITC anti-IgA (5 μg ml^{-1}).The sections were incubated with DAPI (Vector Laboratories), and analysed using a confocal microscope (FV1000-D; Olympus).

Surgical procedure. In appendectomized groups, germ-free mice underwent incision (2 cm in length) on the abdomen under anaesthesia, and the appendix was gently pulled out, ligated with 5-0 Polydioxanone Suture (Ethicon) at the border between the appendix and caecum, and resected in a vinyl isolator. This procedure ensured complete removal of appendix lymphoid tissues and minimized contamination. The caecal stump was irrigated with PBS and the wound was closed. In sham-operated groups, germ-free mice underwent incision of the abdomen and the wound was closed without further treatment. After surgery, mice were maintained under germ-free condition for 1 week. Mice were then transferred to specific-pathogen-free conditions and kept for 2, 4 or 8 weeks (see also Supplementary Figs 2 and 5a). The appendectomized mice were kept separately from the sham-operated mice. Each group was housed in one cage.

Isolation of lymphocytes. To prepare lymphocytes from Peyer's patches and caecal patches, tissues were gently squeezed between glass slides, and the cells were passed through 40 μm nylon meshes. Intestinal lamina propria lymphocytes were prepared as described previously[43]. Briefly, the small and large intestines were opened, washed to remove faecal content, shaken in HBSS containing 5 mM EDTA for 20 min at 37 °C and cut into small pieces, and incubated with RPMI 1640 containing 4% fetal bovine serum (FBS), 1 mg ml^{-1} collagenase D (Roche), 0.5 mg ml^{-1} dispase (Invitrogen) and 40 μg ml^{-1} DNase I (Roche) for 1 h at 37 °C in a shaking water bath. The digested tissues were subjected to Percoll density-gradient (40%/70%) centrifugation. The lamina propria lymphocytes were collected at the interface of the Percoll gradient.

Intracellular cytokine staining. Intracellular expression of IFN-γ, IL-17 and IL-10 in CD4$^+$ T cells was analysed using a Cytofix/Cytoperm Kit Plus (BD Biosciences) according to the manufacturer's instructions. Briefly, lymphocytes obtained from the intestinal lamina propria were incubated with 50 ng ml^{-1} of phorbol myristate acetate (Sigma), 5 μM of calcium ionophore A23187 (Sigma) and Golgistop at 37 °C for 4 h. Cells were incubated with PerCP/Cy5.5 anti-CD4 mAb (2 μg ml^{-1}). After Fix/Perm treatment for 20 min, intracellular cytokine staining was performed with PE anti-IL-10 (2 μg ml^{-1}), FITC anti-IFN-γ (5 μg ml^{-1}) and Alexa Fluor 647 anti-IL-17A(5 μg ml^{-1}) mAbs for 20 min.

Flow cytometry. Cells were treated with anti-CD16/32 mAb (10 μg ml^{-1}) in PBS containing 2% FBS to block nonspecific binding, and incubated with the indicated mAbs. Samples were incubated with 7-amino-actinomycinD (1 μg ml^{-1}) to exclude dead cells before analyses. Flow cytometry was performed using a FACSCanto II flow cytometer (BD Biosciences) with FlowJo software (Tree Star). To measure the absolute number of CD4$^+$ T cell subsets and surface IgA$^+$ cells in the intestine, total number of cells isolated from tissues was counted, and then proportion of each cell population was determined by flow cytometry. The number of CD4$^+$ T cell subsets and surface IgA$^+$ cells was calculated as 'total cell number' × 'percentage in flow cytometry'. For cell isolation, cells were sorted using FACSAria (BD Biosciences).

Measurement of IgA. To prepare faecal samples, faeces were homogenized in PBS (1 mg faeces in 10 ml PBS), and subjected to stepwise centrifugation with increasing force (400 *g* for 5 min, 8,000 *g* for 10 min and 19,000 *g* for 10 min) to remove debris. To prepare mononuclear cells in tissues, Peyer's patches and the caecal patch were shaken for 20 min at 37 °C in HBSS containing 5 mM EDTA to remove epithelial cells. The tissues were digested with 1 mg ml^{-1} Collagenase D (Roche Diagnostics) and applied to a discontinuous 40 and 70% Percoll density gradient (GE Healthcare). The mononuclear cells were then cultured for 3 days and the culture supernatants were collected. IgA levels in the faeces, sera and culture supernatants were determined by a mouse IgA ELISA quantitation kit (Bethyl Laboratories). Optical densities were determined at a wavelength of 450 nm with a reference wavelength of 570 nm.

Extraction of bacterial DNA from faeces. Faeces were collected in collection tubes containing RNA*later* (Ambion). After weighing, RNA*later* was added to make a 10-fold diluted faecal homogenate. The homogenate (200 μl) was washed twice with 1 ml PBS. Glass beads (0.3 g; diameter, 0.1 mm; (BioSpec Products), 300 μl Tris-SDS solution and 500 μl TE-saturated phenol were added to the suspension, and the mixture was vortexed vigorously for 30 s using a FastPrep-24 (MP Biomedicals) at 5.0 power level for 30 s. After centrifugation at 20,000 *g* for 5 min at 4 °C, 400 μl of the supernatant was collected. Subsequently, phenol–chloroform extraction was performed and 250 μl of the supernatant was subjected to isopropanol precipitation. Finally, the DNA was suspended in 200 μl of TE buffer and stored at −20 °C.

Determination of microbiota by 16S rRNA pyrosequencing. PCR was performed using a primer set (784F: 5′-AGGATTAGATACCCTGGTA-3′ and 1061R: 5′-CRRCACGAGCTGACGAC-3′) targeting the V5–V6 region of the 16S rRNA genes[44]. To amplify the targeted region, 1 μl of extracted DNA served as the template in 50 μl reactions using KAPA HiFi HS Ready Mix (KAPA Biosystems). PCR conditions were 95 °C for 3 min, 25 cycles at 98 °C for 20 s, 60 °C for 15 s and 72 °C for 15 s. Two 100-μl three-cycle reconditioning PCR reactions were performed per sample to eliminate heteroduplexes, with 10 μl aliquots of the initial PCR product mixture as the template and other PCR conditions unchanged. Products of the two reconditioning PCR reactions per sample were combined and purified using DNA clean and Concentrator-5 (Zymo Research). Amplified PCR products were used as a template for pyrosequencing with the GS Junior platform (Roche). Pyrosequencing was performed by following the manufacturer's instruction using MID tags. Raw sequences were demultiplexed and quality-trimmed using the QIIME pipeline[45] with default parameters. The trimmed sequences were denoised using AmpliconNoise version 1.2.7 (ref. 46). USEARCH version 6.0.203 (ref. 47) was employed to remove chimaera sequences using the SILVA 111 database[48] as a reference. The processed sequences were then clustered into OTU defined at 97% similarity cutoff using UCLUST version 1.2.22q (ref. 47). Representative sequences for each OTU were classified taxonomically using RDP Classifier version 2.2 (ref. 49) with the SILVA 111 database. Rarefaction curves and UniFrac (ref. 50) distance matrixes were generated using the QIIME tool. The relative abundance was represented as the ratio of the bacterial group to the whole microbiota.

Photoconversion. Kaede bone marrow chimeric mice were generated by intravenous injection of Kaede-labelled bone marrow cells (2×10^6) into 9.5-Gy-irradiated wild-type C57BL/6 mice. Mice were allowed to reconstitute for at least 6 weeks before experimental procedures. For photoconversion, mice were anaesthetized with isoflurane, and a skin incision was made in the abdominal skin to expose Peyer's patches and caecal patches. The surrounding tissue was covered with aluminium foil to prevent unnecessary exposure, and the tissues were exposed to violet light (200 mW cm^{-2}) with a 436-nm g-line band-pass filter with spot UV curing equipment (SP500; Usio) for 5 min. The abdominal wall was closed by 9-mm Autoclips (Clay Adams).

Adoptive transfer experiments. B220$^+$ cells were positively separated using the MACS separation system (Miltenyi Biotec) from Peyer's patches and caecal patches of CD45.2 mice. Sorted cells (1×10^6) were intravenously injected into C57BL/6 CD45.1 recipients through the retro-orbital plexus. Seven days after injection, the lymphocytes were isolated from the small and large intestinal lamina propria and analysed using a flow cytometer.

B-cell activation and coculture with GALT-DCs. To prepare GALT-DCs, C57BL/6 mice were injected s.c. with B16 cells secreting Flt3L as described[51]. After 14 days of the injection, Peyer's patches and caecal patches were isolated and digested with RPMI1640 containing 4% FBS, 1 mg ml^{-1} collagenase D (Roche Diagnostics) and 40 μg ml^{-1} DNase I (Roche Diagnostics) for 30 min at 37 °C. Cells were spun through a 17.5% Accudenz solution (Accurate Chemical & Scientific Corporation).